Electronic Supplementary Material (ESI) for ChemComm.

Validation of a post-radiolabeling bioconjugation strategy for radioactive rare earth complexes with minimal structural footprint

Raphael Lengacher, Alexia G. Cosby, Dariusz Śmiłowicz, Eszter Boros*

Contents

1. General

All starting materials were purchased from commercial sources and used without further purification. **NMR spectra** (^{1}H, ^{13}C) were collected on a 700 MHz Advance III Bruker, 700 MHz, or 400 MHz Bruker instrument in deuterated solvents at 298 K; chemical shifts (δ) in ppm relative to residual solvent resonances ($CDCl_3$ ^{1}H: δ 7.26, ^{13}C: δ 77.16; CD_3CN ^{1}H: δ : 1.96); coupling constants (J) in Hz. Signal assignments are based on coupling constants, increment calculations and/or 2D-NMR experiments. Data was processed using TopSpin 4.1.4. Chemical shifts are reported as parts per million (ppm).

Low resolution electrospray ionization (ESI) mass spectrometry was carried out at the Stony Brook University Institute for Chemical Biology and Drug Discovery (ICB&DD) Mass Spectrometry Facility with an Agilent LC/MSD.

High resolution ESI mass spectrometry was carried out at the Stony Brook University Center for Advanced Study of Drug Action (CASDA) with a Bruker Impact II UHR QTOF MS system.

UV-VIS spectra were collected with the NanoDrop One C instrument. Spectra were recorded from 200 to 900 nm in a quartz cuvette with 1 cm path length.

Luminescence measurements were carried out on a Hitachi F-7100 FL spectrophotometer. Wavelength scans were collected by exciting at the appropriate wavelength (282 for Tb(III)) for antenna-mediated excitation and minimization of scattering interference. Emission spectra were collected from 300 to 800 nm, with 1.0 nm excitation and 5.0 nm emission slit widths, 1200 s scan time, 0.05 s response time, and PMT voltage = 400 V.

ICP-OES was carried out using an Agilent 5110 inductively coupled plasma optical emission spectrometer. A 10-point standard curve or a 6-point standard curve with respect to europium or terbium was used and fits were found to be at least R 2 of 0.999. Concentrations were back calculated to determine the stock sample concentration.

All **HPLC** purification and analytical methods were conducted using a binary solvent system in which solvent A was water + 0.1% TFA and solvent B was MeCN + 0.1% TFA. Preparative HPLC was carried out on a Phenomenex Luna C18 column (250 mm × 21.2 mm, 100 Å, AXIA packed) at a flow rate of 15 mL/min using a Shimadzu HPLC-20AR equipped with a binary gradient pump, UV-vis detector, and manual injector. UV absorption was recorded at 254 nm. Method A: Gradient: 0–1 min: 5% B; 1–14 min: 5–50% B; 14–23 min: 50–95% B; 23–26 min: 95% B; 26–27 min: 95–5% B; 27–30 min: 5% B. Flash chromatography was carried out using a Combi Flash Rf+ on a RediSep column (100 g HP C18 gold, CV: 87.7 mL, flow rate: 60 mL/min). Method B: Gradient: 1-2 min 10% B; 2-3 min: 10–20% B; 3–19 min: 20–25% B; 19 min: 25-100% B; 19-23 min: 100% B; 23 min: 100-10% B; 23-25 min: 10% B. Analytical HPLC was carried out on a Phenomenex Luna 5 µm C18 column (150 mm × 3 mm, 100 Å, AXIA packed) at a flow rate of 0.8 mL/min using either a Shimadzu HPLC-20AR equipped with a binary gradient pump, UV-vis detector, autoinjector, and Laura radiodetector or Agilent 1260 Infinity II HPLC. UV absorption was recorded at 254 nm. Method C: (Shimadzu system) Gradient: 0–2 min: 5% B; 2–14 min: 5–95% B; 14–16 min: 95% B; 16–16.5 min: 95–5% B; 16.5–20 min 5% B. Method D: 0–16 min: 5–95% B

Analytical HPLC traces have been baseline corrected versus a blank measurement (Figure S1).

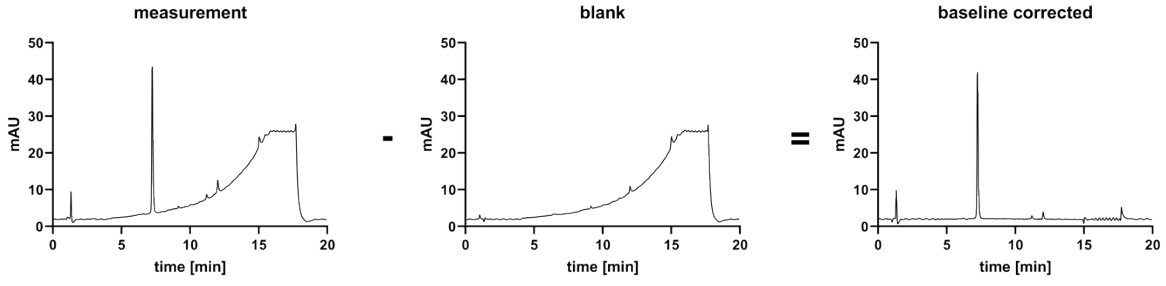

Figure S1: Basline correction of HPLC traces versus a blank measurement on the example of compound **[^{177}Lu][Lu(DO3A-pic-SR$_2$)]$^-$**.

2. Literature

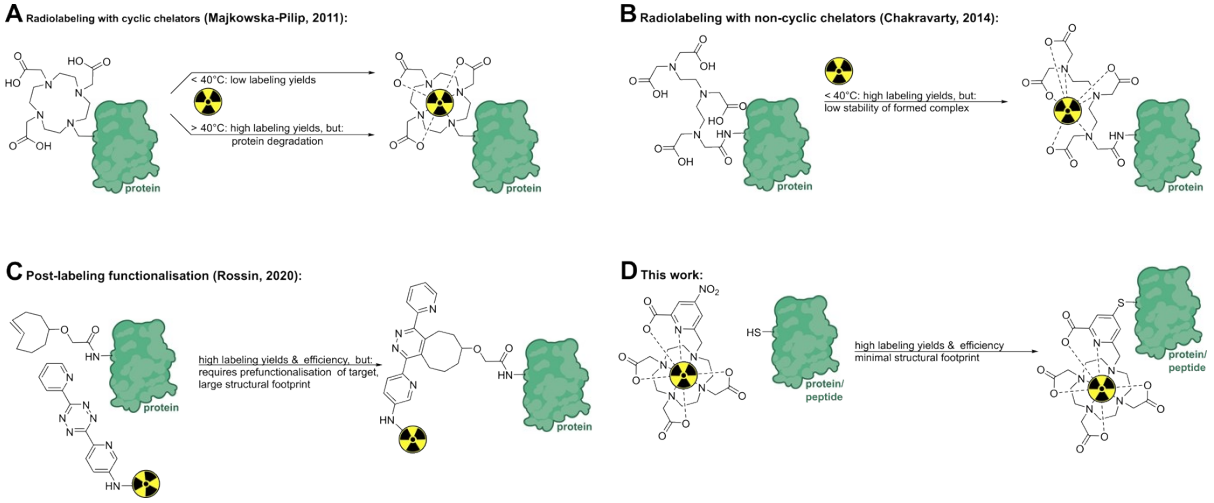

Figure S2: Previous radiolabelling strategies (A-C) and this work (D). **A:** Two-step approach first by conjugation of chelator to protein followed by radiometal coordination. Below 40°C, radiolabeling yields are usually low. **B:** Radiolabeling with non-cyclic chelators leads to good radiolabeling yields below 40°C, but stability of the radiocomplex is impaired, leading to loss of radioactive payload in vivo. **C:** Post-labeling strategy based on a tetrazine and trans-cyclooctene click reaction. This leads to high yields, but results in a big structural footprint and requires modification of the targeting vector. **D:** Post-labeling strategy presented in this work. This strategy incorporates high radiolabeling yields and produces a minimal structural footprint.

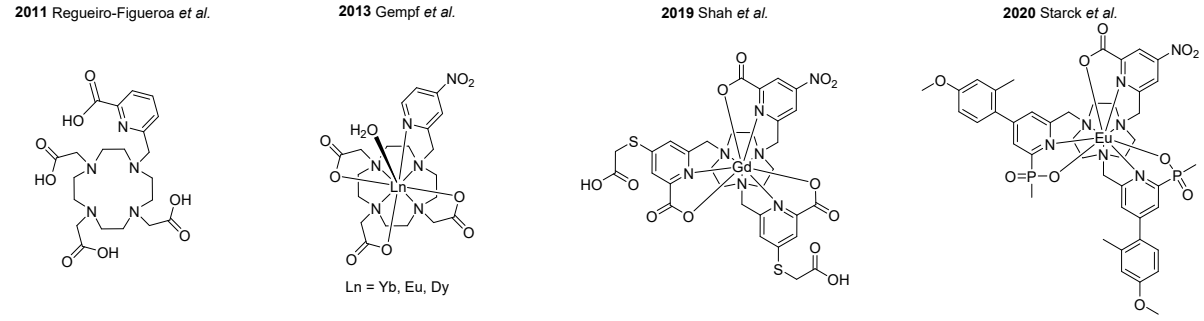

First reported DO3Apic synthesis
DOTA analogue with q = 0

First report of cysteine selective conjugation
Conjugation to small peptides and BSA
Used as luminescent probes

Gd spin label conjugated to protein
homo dimer TRIM25cc
used in nanometer-distance measurements by EPR

Luminescent probe conjugated to a ER targeting peptide

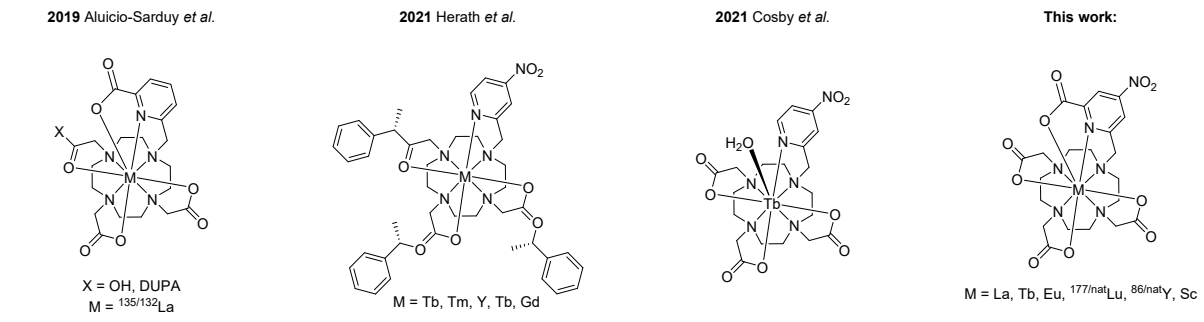

DO3Apic as chelator for radiometals and DUPA induced targetting of PSMA positive cancer cells *in vivo*

Chiral Lanthanide tag as tool to probe proteins with multiple spectroscopic techniques such as NMR, EPR, and FRET

Tb(DO3Apic) as luminescent probe for H_2S detection

DO3Apic-NO2 for the introduction of rare-earth radioisotopes to biologic targeting vectors

Figure S3: Summary on previous work on the DO3Apic scaffold compared to this work.

3. Synthesis

The synthesis of **DO3A-pic-NO_2** was carried out according to a slightly modified procedure from literature.[1]

Synthesis of S1

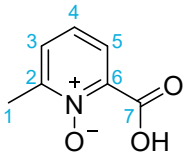

6-Methyl-pyridine-2-carboxylic acid (2.00 g, 14.5 mmol, 1 equiv.) was dissolved in anhydrous CH_2Cl_2 (10 mL) at r.t., followed by addition of urea hydrogen peroxide (4.12 g, 43.8 mmol, 3 equiv.). The mixture was placed in an ice bath (0°C) and trifluoracetic acid anhydride (6.18 mL, 43.7 mmol, 3 equiv.) was added dropwise. The solution was stirred at r.t. for 4 h, followed by addition of Na_2SO_4 (aq., sat.). The resulting solution was extracted with CH_2Cl_2. The combined organic phases were dried over Na_2SO_4, filtered, and concentrated *in vacuo*, providing the title compound **S1** as a clear crystalline solid (1.58 g, 10.3 mmol, 71%), which was used without further purification in the next step. **^{1}H NMR** ($CDCl_3$, 700 MHz): δ 8.33 (dd, 1H, *J* = 7.29, 2.25 Hz, H_4), 7.60-7.51 (m, 2H, $H_{3,5}$), 2.65 (s, 3H, H_1). **^{13}C NMR** ($CDCl_3$, 175 MHz): δ 161.61 (C_q, 1 C, C_7), 149.31 (C_q, 1 C, C_2), 137.06 (C_q, 1 C, C_6), 129.97 (CH_1, 1 C, $C_{3/5}$), 129.82 (CH_1, 1 C, $C_{5/3}$), 127.29 (CH_1, 1 C, C_4), 17.65 (CH_3, 1 C, C_1). **HR-ESI-MS:** $[M+H]^+$ = calc. m/z 154.0499, found: m/z 154.0500

Synthesis of S2

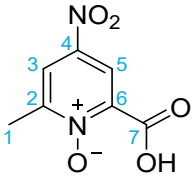

Concentrated H_2SO_4 (34.6 mL, 650 mmol) was added dropwise to **S1** (5.38 g, 35 mmol) at -10°C (acetone/ice bath) while stirring. After 30 min, concentrated (70%) HNO_3 (44 mL, 734 mmol) was added dropwise over 18 min. The resulting slurry was brought to 110°C over 3 h. The reaction was stirred at 110°C for 3 days. The solution was allowed to cool to r.t. and then added slowly (over 1 h) to 400 mL ice, resulting in formation of a precipitate. The precipitate was filtered and dried, providing the title compound **S2** as a colourless solid (2.34 g, 11.8 mmol, 34%). **^{1}H NMR** (CD_3CN, 700 MHz): δ 8.79 (d, 1H, *J* = 3.14 Hz, H_4), 8.48 (d, 1H, *J* = 3.12 Hz, H_3), 2.65 (s, 1H, H_1). **^{13}C NMR** (CD_3CN, 175 MHz): δ 160.02 (C_q, 1 C, C_7), 152.69 (C_q, 1 C, C_2), 145.15 (C_q, 1 C, C_4), 138.37 (C_q, 1 C, C_6), 123.65 (CH_1, 1 C, C_5), 120.54 (CH_1, 1 C, C_3), 17.05 (CH_3, 1 C, C_1). **HR-ESI-MS:** $[M+H]^+$ = calc. m/z 199.0349, found: m/z 199.0351

Synthesis of S3

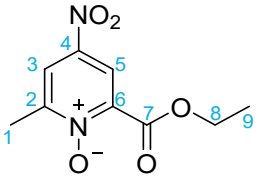

Anhydrous EtOH (32 mL, 140 equiv.) was added to **S2** (785.6 mg, 3.96 mmol, 1 equiv.) at r.t.. Concentrated H_2SO_4 (0.85 mL, 1.59 mmol, 0.4 equiv.) was added and the solution was heated to 85°C for 3 d. The solution was allowed to cool to r.t., washed with $NaHCO_3$ (aq., 5 wt%, 2×), dried over Na_2SO_4 and concentrated *in vacuo*, providing the title compound **S3** as a yellow solid (668.0 mg, 2.95 mmol, 74%). **^{1}H NMR** ($CDCl_3$, 700 MHz): δ 8.30 (s, 1H, H_5), 8.18 (s, 1H, H_3), 4.50 (q, 2H, *J* = 6.94 Hz, H_8), 2.57 (s, 3H, H_1), 1.43 (t, 3H, *J* = 6.46 Hz, H_9). **^{13}C NMR** ($CDCl_3$, 175 MHz): δ 160.14 (C_q, 1 C, C_7), 152.43 (C_q, 1 C, C_6), 142.37 (C_q, 1 C, C_2), 140.37 (C_q, 1 C, C_4), 121.10 (CH_1, 1 C, C_5), 118.87 (CH_1, 1 C, C_3), 63.29 (CH_2, 1 C, C_8), 18.19 (CH_2, 1 C, C_1), 14.07 (CH_3, 1 C, C_9). **HR-ESI-MS:** $[M+H]^+$ = calc. m/z 227.0662, found: m/z 227.0664. Analytical data matches that reported previously.[1]

Synthesis of S4

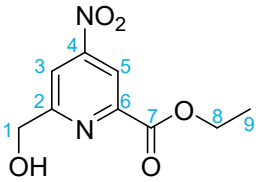

Anhydrous $CHCl_3$ (10 mL) was added to **S3** (64.0 mg, 0.28 mmol, 1 equiv.) at r.t.. Trifluoroacetic acid anhydride (0.8 mL, 5.7 mmol, 20 equiv.) was added dropwise at r.t., and the resulting mixture was heated to 60°C for 4.5 h. The solvent was evaporated. The residual material was redissolved in EtOH/H_2O (1:1, 20 mL) and stirred at r.t. for 3 h. EtOH was evaporated and the aqueous solution was extracted with CH_2Cl_2 (200 mL, 3×). The combined organic phases were dried over Na_2SO_4 and concentrated *in vacuo*, providing the title compound **S4** as a dark yellow solid (59.6 mg, 0.28 mmol, 99%) used without further purification.**^{1}H NMR** (CD_3CN, 700 MHz): δ 8.52 (s, 1H, H_5), 8.34 (s, 1H, H_3), 4.86 (s, 2H, H_1), 4.65 (q, *J* = 6.61 Hz, H_8), 1.42 (t, *J* = 6.50 Hz, H_9).**^{13}C NMR** (CD_3CN, 175 MHz): δ 165.94 (C_q, 1 C, C_7), 163.44 (C_q, 1 C, C_6), 155.72 (C_q, 1 C, C_4), 150.17 (C_q, 1 C, C_2), 115.90 (CH_1, 1 C, C_5), 115.81 (CH_1, 1 C, C_3), 63.96 (CH_2, 1 C, C_1), 62.28 (CH_2, 1 C, C_8), 13.46 (CH_3, 1 C, C_9). **HR-ESI-MS:** $[M+H]^+$ = calc. m/z 227.0662, found: m/z 227.0664

Synthesis of DO3A-pic-NO_2

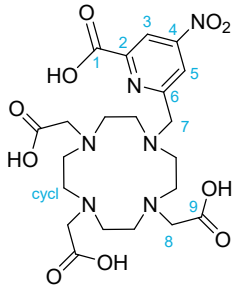

Ethyl 6-(hydroxymethyl)-4-nitropicolinate **S4** (59.0 mg, 0.26 mmol, 1 equiv.) was dissolved in anhydrous THF (10 mL) and placed under a N_2 atmosphere at 0°C. Anhydrous triethyl amine (109 µL, 0.78 mmol, 3 equiv.) was added, followed by dropwise addition of methanesulfonyl chloride (30.3 µL, 0.39 mmol, 1.5 equiv.). The reaction was stirred at 0°C for 30 min, followed by 1.5 h at r.t.. The mixture was concentrated, redissolved in CH_2Cl_2, washed consecutively with water and brine, dried over Na_2SO_4, and concentrated *in vacuo*, providing the title compound **S5** as a yellow oil used without purification in the next step.

Ethyl 6-(((methylsulfonyl)oxy)methyl)-4-nitropicolinate **S5** (80.0 mg, 0.26 mmol, 1 equiv.) was dissolved in anhydrous acetonitrile and added dropwise to a solution of ^{t}Bu-DO3A (135.3 mg, 0.26 mmol, 1 equiv.) and K_2CO_3 (181 mg, 1.32 mmol, 5 equiv.) in anhydrous acetonitrile (10 mL). The mixture was heated to reflux for 2 h, filtered, and concentrated *in vacuo* yielding crude product used without purification (71.1 mg, 0.098 mmol). ESI-MS calcd. for $C_{35}H_{58}N_6O_{10}$: 722.42. Found: 723.2 $[M+H]^+$. The protected macrocycle was then treated with 1.0 M NaOH (2 mL) and stirred overnight at r.t.. Following acidification to pH 2 with 15% HCl, the product was purified via semipreparative HPLC, the fractions containing product were pooled and the solvent was removed *in vacuo* and then immediately treated with TFA/CH_2Cl_2 (2:1) and stirred at r.t. overnight. The crude material was purified using semipreparative HPLC (Rt = 10.1 min). Fractions containing pure material were collected, lyophilized, and immediately stored at -80°C to preserve material integrity (8.6 mg, 0.026 mmol). **^{1}H NMR** (CD_3OD, 400 MHz): δ 8.68 (s, 1H, H_3), 8.56 (d, 1H, H_5), 4.45 (br s, 2H, H_7), 3.98 (m, 6H, H_8), 3.56-3.17 (m, 16H, H_{cycl}). **HR-ESI-MS:** $[M+H]^+$ = calc. m/z 527.2096, found: m/z 527.2087

Synthesis of **[RE(DO3A-pic-NO$_2$)]$^-$** complexes

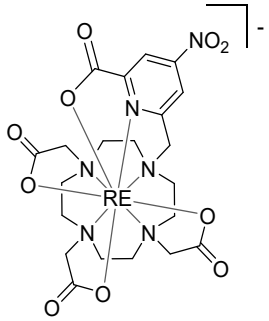

RE^{3+}-salts (40 µmol, 2 equiv.) were added to a solution of **DO3A-pic-NO$_2$** (20 µmol, 1 equiv.) in MeOH/H_2O (1:1, pH = 6.5) and the resulting solution was stirred at r.t. overnight. The solution was lyophilized and the remaining solids were purified by SepPak. Yields were determined by ICP-OES.

[La(DO3A-pic-NO$_2$)]$^-$: Ln^{3+}-salt: $LaCl_3$, isolated yield after SepPak: 2240.1 nmol, 11%

HR-ESI-MS: $[M+2H]^+$ = calc. m/z 663.0925, found: m/z 663.0929

HPLC (Method C): R_t = 2.27 min.

[Tb(DO3A-pic-NO$_2$)]$^-$: Ln^{3+}-salt: $TbOTf_3$, isolated yield after SepPak: 970.7 nmol, 5%

HR-ESI-MS: $[M]^-$ = calc. m/z 681.0964, found: m/z 681.0978

HPLC (Method C): R_t = 2.03 min.

[Eu(DO3A-pic-NO$_2$)]$^-$: Ln^{3+}-salt: $EuOTf_3$, isolated yield after SepPak: 132.7557 nmol, 1%

HR-ESI-MS: HR-ESI-MS: $[M]^-$ = calc. m/z 675.0928, found: m/z 675.0944

HPLC (Method C): R_t = 2.13 min.

[Lu(DO3A-pic-NO$_2$)]$^-$: Ln^{3+}-salt: $LuCl_3 \cdot 6\ H_2O$, isolated yield after SepPak: 1313.2 nmol, 7%

HR-ESI-MS: $[M+2H]^+$ = calc. m/z 699.1269, found: m/z 699.1270

HPLC (Method C): R_t = 1.62 min.

[Sc(DO3A-pic-NO$_2$)]$^-$: Ln^{3+}-salt: $ScCl_3 \cdot 6\ H_2O$, isolated yield after SepPak: 476.4 nmol, 2%

HR-ESI-MS: $[M+2H]^+$ = calc. m/z 569.1421, found: m/z 569.1415

[Y(DO3A-pic-NO$_2$)]$^-$: Ln^{3+}-salt: $Y(NO_3)_3 \cdot 6\ H_2O$, isolated yield after SepPak: 617.4 nmol, 3%

HR-ESI-MS: $[M+2H]^+$ = calc. m/z 613.0920, found: m/z 613.0917

HPLC (Method C): R_t = 1.98 min.

Synthesis of [Lu(DO3A-pic-SR_2)]$^-$

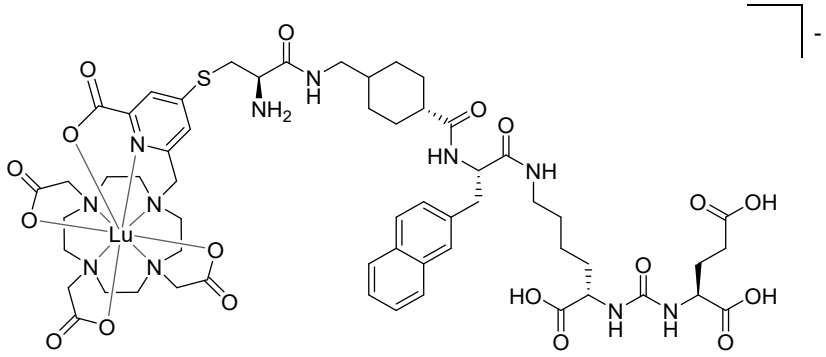

(((1S)-5-((2S)-2-(4-(((R)-2-amino-3-mercaptopropanamido)methyl)cyclohexane-1-carboxamido)-3-(naphthalen-2-yl)propanamido)-1-carboxypentyl)carbamoyl)-L-glutamic acid (30 nmol, 1 equiv.) was added to a solution of TCEP·HCl (37.5 nmol, 1.25 equiv.) and **[Lu((DO3A-pic-NO_2))]$^-$** (30 nmol, 1 equiv.) in 25 mM NH_4HCO_3 buffer at pH 7.5 (700 µL). The resulting solution was left on a shaker at r.t. overnight. The title compound was isolated from the crude reaction mixture by HPLC purification and identified by HR-ESI-MS. HR-ESI-MS: $[M+2H]^+$ = calc. m/z 1410.4571, found: m/z 1410.4571. HPLC (Method C): R_t = 7.25 min.

Synthesis of [Y(DO3A-pic-SR_2)]$^-$

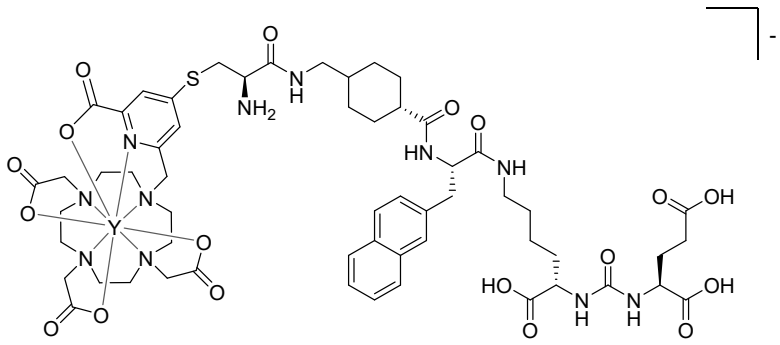

(((1S)-5-((2S)-2-(4-(((R)-2-amino-3-mercaptopropanamido)methyl)cyclohexane-1-carboxamido)-3-(naphthalen-2-yl)propanamido)-1-carboxypentyl)carbamoyl)-L-glutamic acid (300 nmol, 5 equiv.) was added to a solution of TCEP·HCl (375 nmol, 6.25 equiv.) and **[Y(DO3A-pic-NO_2)]$^-$** (60 nmol, 1 equiv.) in 25 mM NH_4HCO_3 buffer at pH 7.5 (317 µL). The resulting solution was incubated at r.t. overnight. The title compound was isolated from the crude reaction mixture by HPLC purification and identified by HR-ESI-MS. HR-ESI-MS: $[M+3H]^{2+}$ = calc. m/z 662.7135, found: m/z 662.7147. HPLC (Method C): R_t = 7.27 min.

Conjugation of $[La(DO3Apic\text{-}NO_2)]^-$ to BSA

To a solution of $[La(DO3Apic\text{-}NO_2)]^-$ (166 nmol, 100 equiv.) in $(NH_4)(HCO_3)$ buffer (52 µL, 25 mM, pH = 7.4) was added a solution of BSA (1.66 nmol, 1 equiv.) in $(NH_4)(HCO_3)$ buffer (40 µL, 25 mM, pH = 7.4). The resulting solution was incubated at 37°C for 21 h. The solution was desalted using a Zeba® size exclusion Spin Desalting column and analyzed by MALDI-TOF MS, revealing a signal at 67072 m/z, compared to the signal of unmodified BSA at 66639 m/z, corresponding to the conjugation of a single Lanthanum complex to BSA.

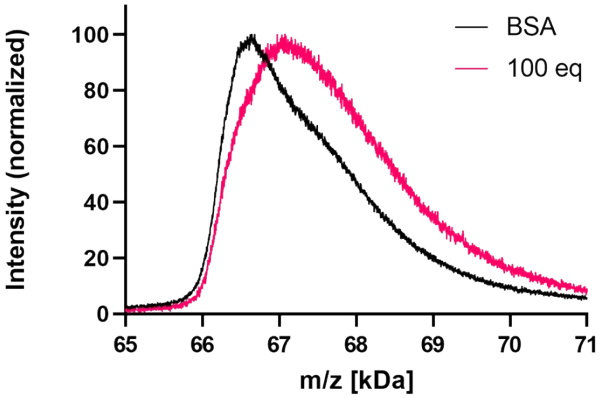

Figure S4: MALDI-TOF MS signals of unmodified BSA (black) and BSA reacted with 100 equivalents of $[La(DO3Apic\text{-}NO_2)]^-$ (red), indicating the conjugation of BSA to a single Lanthanum complex.

4. Kinetic Studies

UV/Vis measurements

Kinetic measurements were carried out following the characteristic shift in UV absorbance from 300 nm to 280 nm as reported in literature.[2] The device was blanked with the corresponding metal complex (30 nmol, 1 equiv.) in 25 mM NH_4HCO_3 buffer at pH 7.5 in a total volume of 694.5 µL. Ethyl thioglycolate (30 nmol in 4.5 µL buffer, 1 equiv.) was added and the reaction progress was monitored every 5 min for a total of 18 h (or 6 h in the case of Sc). The procedure was identical in the case of **DO3A-pic-NO_2**. Curve fits were carried out using exponential decay considering pseudo first order kinetics with GraphPad Prism 9.4.1. Data acquisition was conducted until the reaction produced plateau absorbance for at least 100 minutes.

Table S1: Table summarizing rate constants and half-lives of the conjugation reaction.

M	k [h^{-1}]	$t_{1/2}$ [h]
Ø	0.33 ± 0.01	3.0 ± 0.06
La	0.18 ± 0.01	5.5 ± 0.06
Tb	0.25 ± 0.01	4.0 ± 0.08
Eu	0.31 ± 0.01	3.2 ± 0.04
Lu	0.22 ± 0.01	4.5 ± 0.12
Y	0.25 ± 0.01	4.0 ± 0.03
Sc	0.89 ± 0.03	1.1 ± 0.04

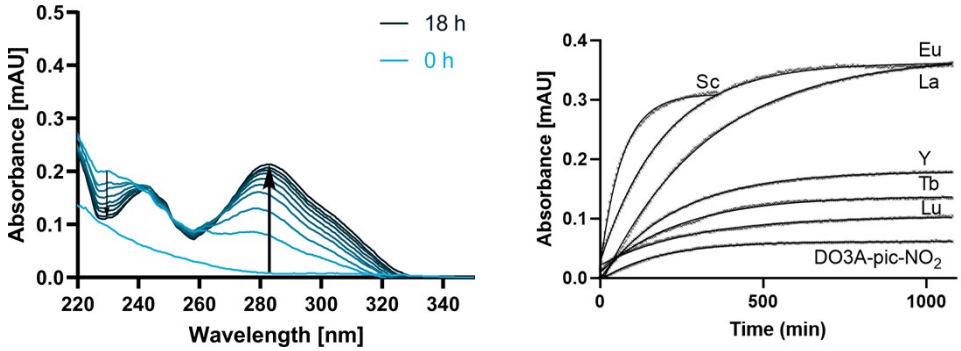

Figure S5: Characteristic shift in UV/Vis spectrum during the thioconjugation reaction, exemplified by the reaction from [Y(**DO3A-pic-NO_2**)]$^-$ to [Y(**DO3A-pic-SR_1**)]$^-$. Kinetic data was obtained by monitoring the increased absorption at 280 nm (left). Kinetic measurements plotting shift in UV absorption at 280 nm versus time (right).

The identity of the **[RE(DO3A-pic-SR_1)]$^-$** complexes was additionally verified by HR-ESI-MS:

[La(DO3A-pic-SR_1)]$^-$: HR-ESI-MS: $[M+2H]^+$ = calc. m/z 736.1157, found: m/z 736.1164

HPLC (Method C): R_t = 5.52 min.

[Tb(DO3A-pic-SR_1)]$^-$: HR-ESI-MS: $[M+2H]^+$ = calc. m/z 756.1347, found: m/z 756.1349

HPLC (Method C): R_t = 5.40 min.

[Eu(DO3A-pic-SR_1)]$^-$: HR-ESI-MS: $[M+2H]^+$ = calc. m/z 750.1306, found: m/z 750.1305

HPLC (Method C): R_t = 5.42 min.

[Lu(DO3A-pic-SR_1)]$^-$: HR-ESI-MS: $[M+2H]^+$ = calc. m/z 772.1501, found: m/z 772.1499

HPLC (Method C): R_t = 5.42 min.

[Y(DO3A-pic-SR_1)]$^-$: HR-ESI-MS: $[M+2H]^+$ = calc. m/z 686.1152, found: m/z 686.1152

HPLC (Method C): R_t = 5.50 min.

DO3A-pic-SR_1: HR-ESI-MS: $[M+H]^+$ = calc. m/z 600.2334, found: m/z 600.2330

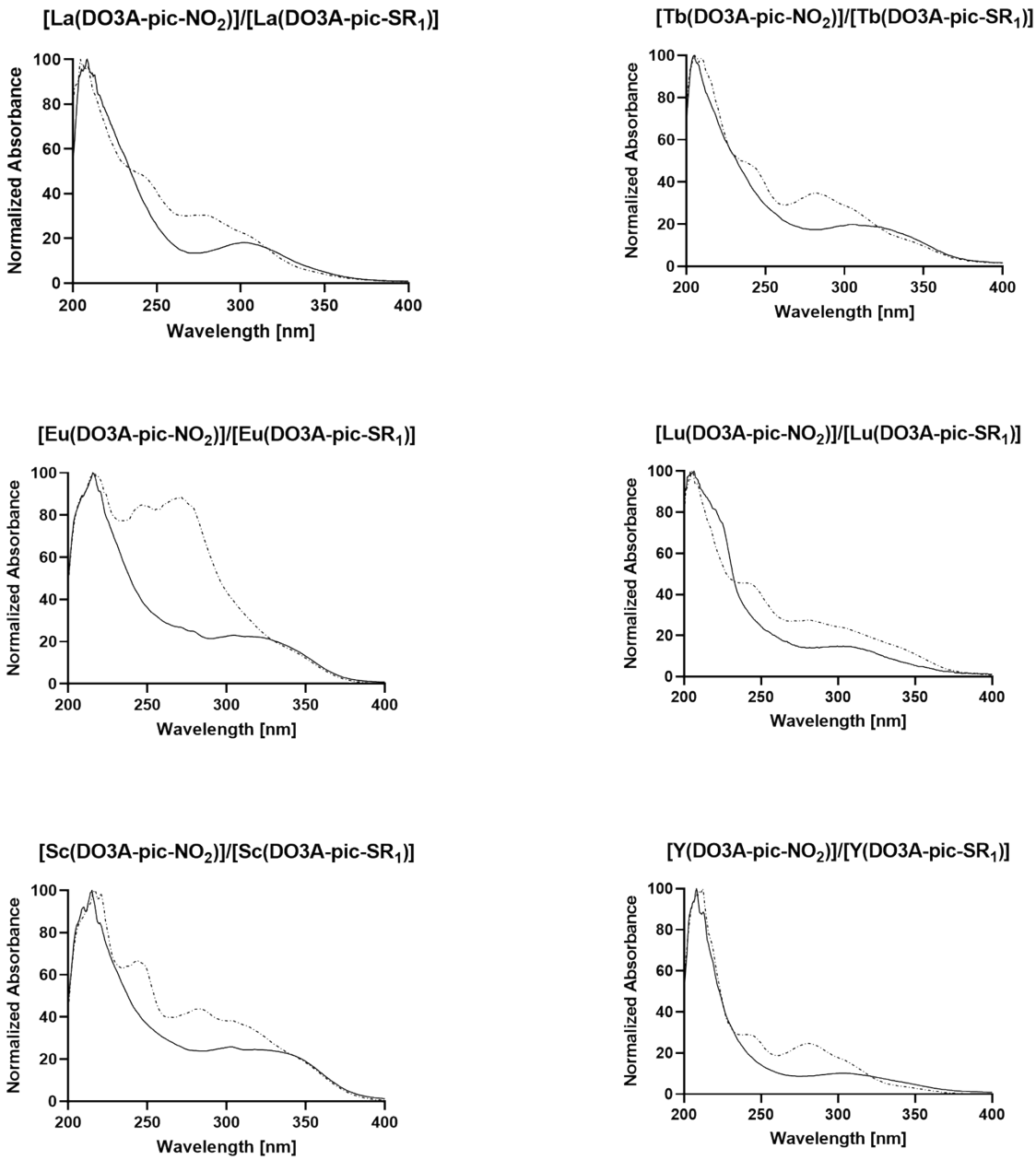

Figure S6: UV/Vis spectra of the investigated **[RE((DO3A-pic-NO_2))]**$^-$ complexes overlayed with their corresponding **[RE((DO3A-pic-SR_1))]**$^-$ complexes.

Luminescence turn-on measurements

Luminescence turn-on measurements were carried out according to the same procedure as UV/Vis measurements. The change in intensity of luminescence emission was monitored for 493, 548, 589, and 625 nm. The k-value was averaged over all observed wavelengths.

In brief, Lifetime values were extracted by fitting the luminescent decay curves with the equation:

$$I_t = I_0 * \exp\left(-\frac{x}{\tau}\right) \quad \text{(S1)}$$

where I_t is the initial luminescent emission intensity, I_0 is the intensity at time x = 0, and τ is the luminescence lifetime. Data was fit using Prism. Q was calculated using Horrocks' method, eq. S2.

$$q = 5.0\left(\frac{1}{\tau(H_2O)} - \frac{1}{\tau(D_2O)} - 0.06\right) \quad \text{(S2)}$$

Table S2: Photophysical properties of [Tb(**DO3A-pic-NO$_2$**)]$^-$ and [Tb(**DO3A-pic-SR$_1$**)]$^-$. q = inner-sphere hydration.[3] Φ determined using reference compound [Tb(**DO3A-pic**)]$^-$.[4]

	[Tb(**DO3A-pic-NO$_2$**)]$^-$	[Tb(**DO3A-pic-SR$_1$**)]$^-$
λ_{ex} [nm]	304	280
q	0	0
Φ [%]	4.7	41

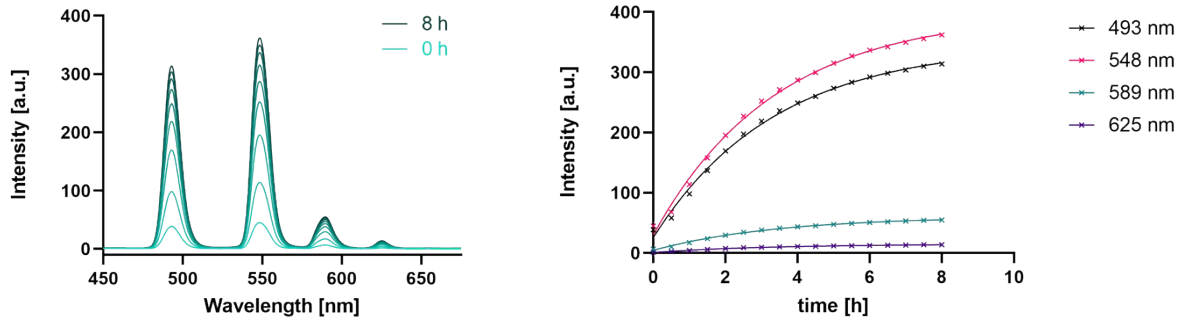

Figure S7: Left: Luminescence turn-on during the thioconjugation reaction from [Tb(**DO3A-pic-NO$_2$**)]$^-$ to [Tb(**DO3A-pic-SEtCOOEt**)]$^-$. Upon conjugation, increased emission from the characteristic Tb emission bands at 493, 548, 589, and 625 nm is observed. **Right:** Luminescence turn-on kinetics of **[Tb(DO3A-pic-NO$_2$)]$^-$** upon thioether formation. Conditions: To [Tb(**DO3A-pic-NO$_2$**)]$^-$ (30 nmol, 1 equiv.) in 25 mM NH_4HCO_3 buffer at pH 7.5 in a total volume of 694.5 µL was added HSR_1 (30 nmol in 4.5 µL buffer, 1 equiv.) and the reaction progress was monitored every 30 min for a total of 8 h. Excitation wavelength = 282 nm.

5. Radiochemistry

Luthetium-177 was received from the University of Missouri through the Department of Energy Isotope Program, in the form of a $^{177}LuCl_3$ solution (pH 2). Yttrium-86 was received from the Engle Group at the University of Wisconsin-Madison, in the form of an $^{86}YCl_3$ solution (pH 2).

Radiolabelling experiments were carried out in triplicate at 80°C with various amounts of chelator (10 nmol, 2.5 nmol, 1 nmol, 0.25 nmol, 0.1 nmol) in 0.25 M NH_4OAc buffer at pH = 5.5 and 30-32 μCi of ^{177}Lu/24-32 μCi of ^{86}Y in a total amount of 116 μL solution.

Apparent Molar Activity

The time-dependent complexation yield for each radioisotope/ligand ratio and the DTPA challenge stability were determined by radio thin-layer chromatography (radio-TLC) using aluminium-backed normal-phase (silica) TLC plates as the stationary phase and 0.15 M NH_4OAc/10 mM EDTA pH 5.0 mixed 1:1 with MeOH as the mobile phase. Under these conditions, free radiometals move with the solvent front (R_f = 0.5–1.0) and complexed radioisotope remains at R_f = 0.1–0.5. Radioactivity distribution on TLC plates was visualized on photo plates with an Amersham Biosciences Typhoon 9400 Variable Mode Imager and quantified using ImageQuant 5.2 software.

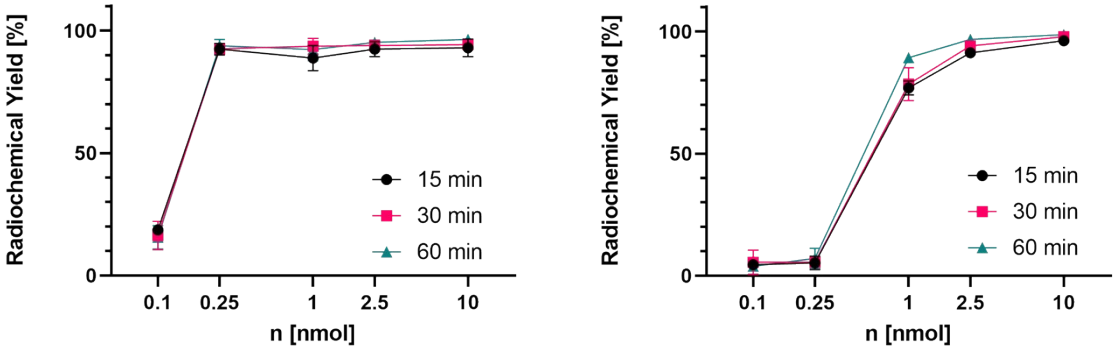

Figure S8: Radiolabelling (triplicate) of [^{177}Lu][**Lu(DO3A-pic-NO_2)**]$^-$ (left) and [^{86}Y][**Y(DO3A-pic-NO_2)**]$^-$ (right) at various ligand concentrations and time points. Conditions: 80°C, pH 5.5, 30-32 μCi ^{177}Lu/24-32 μCi ^{86}Y per sample, 116 μL total volume per sample.

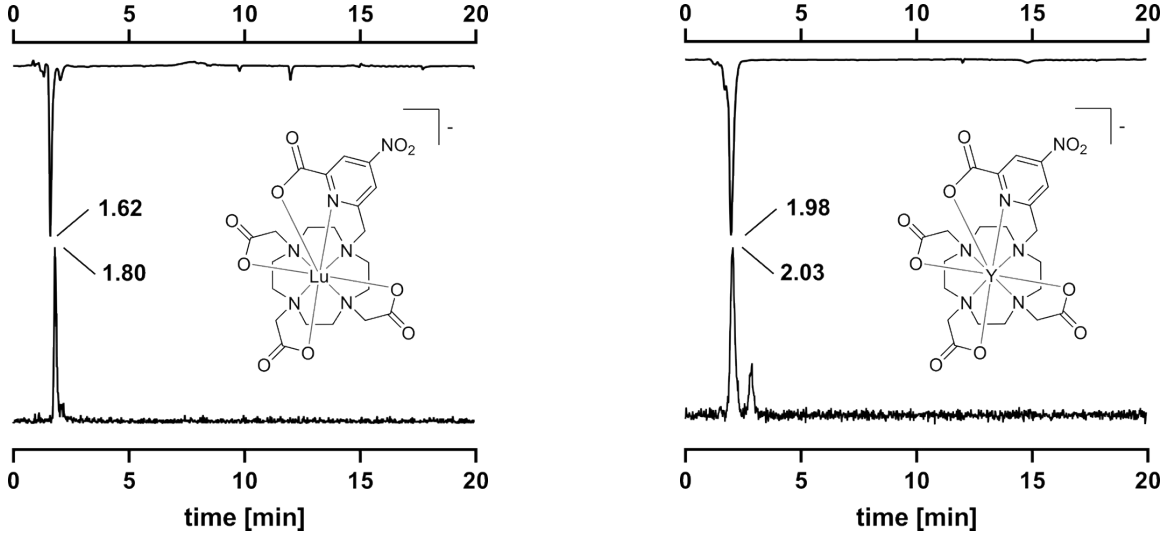

Figure S9: Coinjection of [^{177}Lu][**Lu(DO3A-pic-NO_2)**]$^-$ with its ^{nat}Lu homologue (left) and of and [^{86}Y][**Y(DO3A-pic-NO_2)**]$^-$ and its ^{nat}Y homologue (right). UV trace inverted on top and γ-trace at the bottom.

The signal at 2.93 min is assumed to be a protonation or conformation isomer of the same compound, as it disappears later. Furthermore, collection and reinjection of the first peak again delivers two signals.

DTPA Challenge

^{177}Lu: Following radiolabelling, a 10 mM DTPA/0.25 M NH_4OAc solution at pH 5.5 (10 μL) was added to conjugates in solution (50 μL, 1.04 nmol ligand, n = 3). The final ligand/DTPA molar ratio was 1:300. The resulting solutions were incubated at room temperature for 0.25–24 h. A total of 2 μL was removed at each time point and spotted onto a TLC strip.

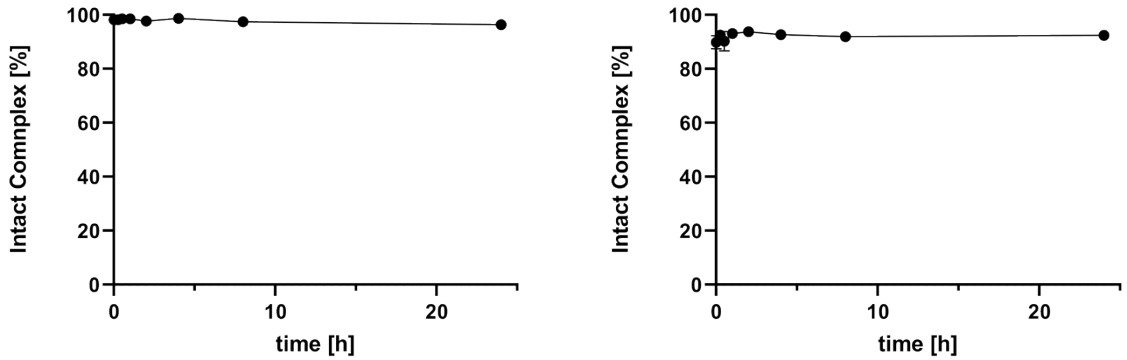

Figure S10: DTPA challenge experiments (triplicate) of [^{177}Lu][**Lu(DO3A-pic-NO_2)**]$^-$ and [^{177}Lu][**Lu(DO3A-pic-SR_1)**]$^-$ over time.

^{86}Y: Following radiolabelling, a 10 mM DTPA/0.25 M NH_4OAc solution at pH 5.5 (10 μL) was added to conjugates in solution [^{86}Y][**Y(DO3A-pic-NO_2)**]$^-$ (0.33 nmol in 36 μL, n = 3) The final ligand/DTPA molar ratio was 1:300. The resulting solutions were incubated at room temperature for 0.25–24 h. A total of 2 μL was removed at each time point and spotted onto a TLC strip.

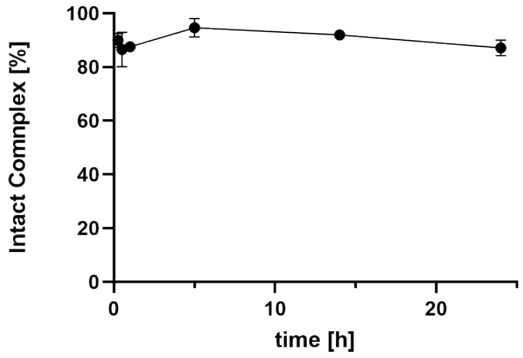

Figure S11: DTPA challenge experiment (triplicate) of [^{86}Y][**Y(DO3A-pic-NO_2)**]$^-$ over time.

Thioconjugation experiments using radioactive species

^{177}Lu: To [^{177}Lu][**Lu(DO3A-pic-NO$_2$)**]$^-$ was added 0.5 M NH_4HCO_3 solution at pH 7.5 (50 µL) and the corresponding thiole (30 eq, 4.5 µL 25 mM NH_4HCO_3 solution at pH 7.5). In the case of peptide conjugation, 37.5 eq. TCEP was added to avoid disulfide formation. The resulting solution was incubated at 37°C. Reaction progress was monitored by radio HPLC.

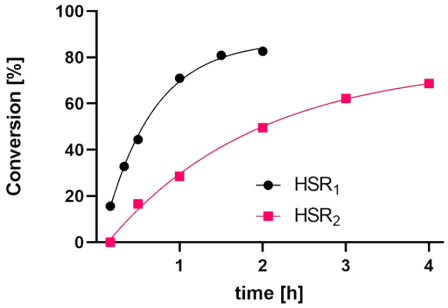

Figure S12: Reaction progress of the thioconjugation between [^{177}Lu][**Lu(DO3A-pic-NO$_2$)**]$^-$ and different thioles over time. Conversion is based on integrated signals of the radiotrace.

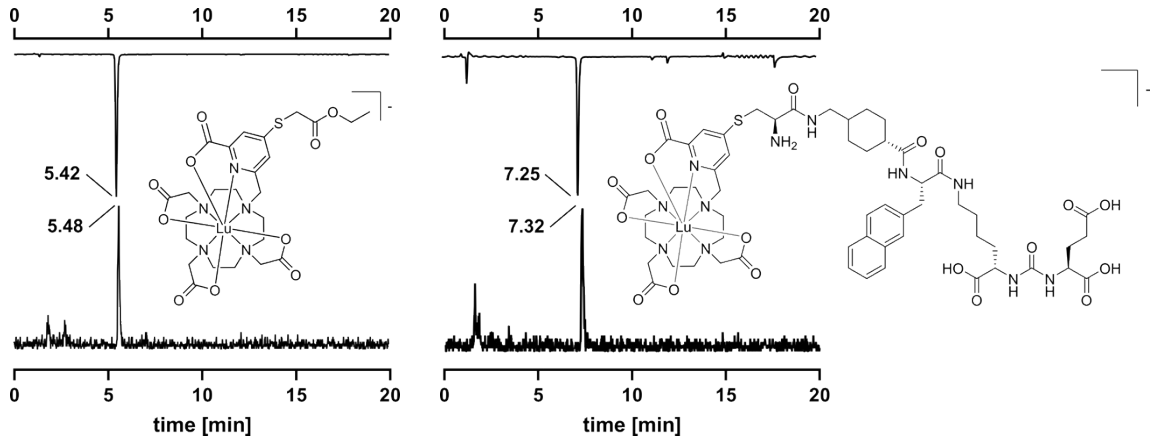

Figure S13: Coinjections of [^{177}Lu][**Lu(DO3A-pic-SEtCOOEt)**]$^-$ (left) and [^{177}Lu][**Lu(DO3A-pic-S-Cys-PSMA)**]$^-$ (right) with their ^{nat}Lu homologues. UV trace inverted on top and γ-trace at the bottom.

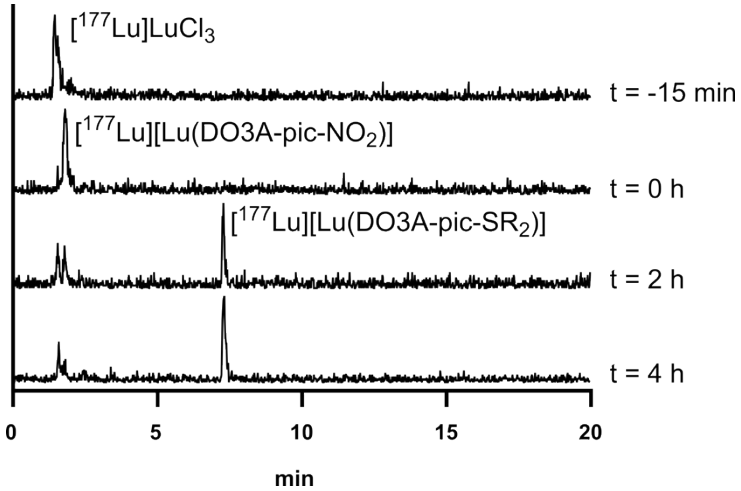

Figure S14: RadioHPLC monitoring of the reaction progress from the radiolabeling of **DO3A-pic-NO$_2$** (t = -15 min to t = 0h) to the formation of [^{177}Lu][Lu(**DO3A-pic-S-Cys-PSMA**)]$^-$ at t = 4 h (normalized).

^{86}Y: To [^{86}Y][**Y(DO3A-pic-NO$_2$)**]$^-$ (5 nmol, pH 5.5) was added 0.5 M NH_4HCO_3 solution at pH 7.5 (50 µL) and HSR_2 (5 eq, 14.4 µL 1.75 mM aqueous solution). 37.5 eq. TCEP (25 nmol, 5 eq, 1 mM in 25 mM NH_4HCO_3 solution at pH 7.5) was added to avoid disulfide formation. The resulting solution was incubated at 37°C. Reaction progress was monitored by radio HPLC.

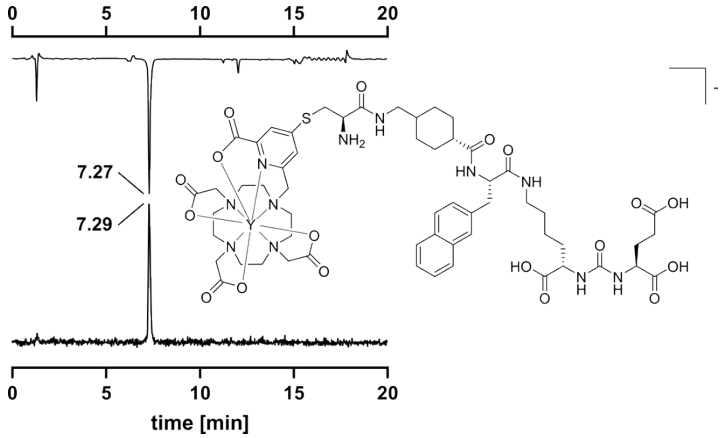

Figure S15: Coinjection of [^{86}Y][**Y(DO3A-pic-SR$_2$)**]$^-$ with its ^{nat}Y homologue. UV trace inverted on top and γ-trace at the bottom.

CRET Plate imaging

An amount of 17-18 µCi of [^{177}Lu][**Lu(DO3A-pic-NO$_2$)**]$^-$ in 8 µL (taken directly from the coupling reaction) was added to various amounts of [**Tb(DO3A-pic-NO$_2$)**]$^-$ and [**Tb(DO3A-pic-SEtCOOEt)**]$^-$ in in 200 µL of 25 mM NH_4HCO_3 solution at pH 7.5. The resulting solutions were imaged on an IVIS Lumina Series III from Caliper LifeSciences small animal imager. Scans were collected over 5 minutes with blocked excitation and open emission filter.

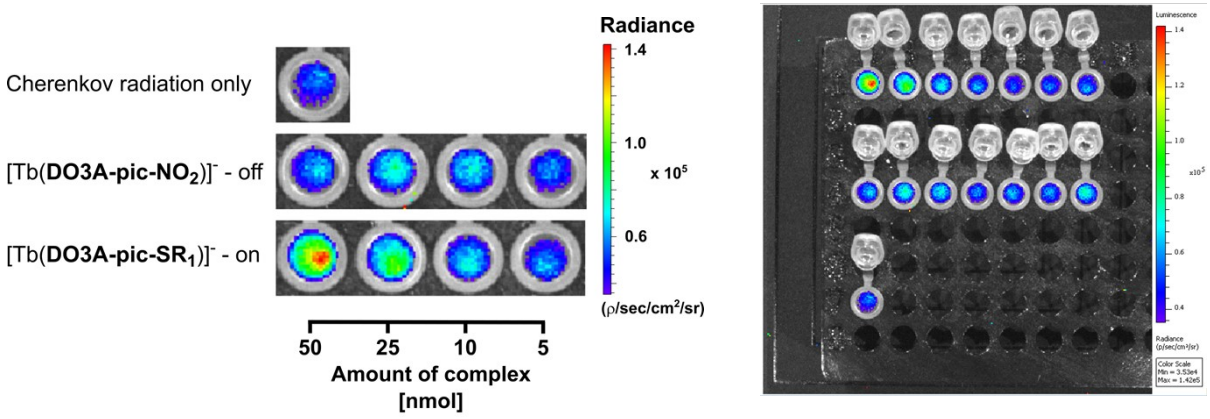

Figure S16: Cherenkov radiation mediated energy transfer (CRET) based luminescence of [Tb(**DO3A-pic-NO$_2$**)]$^-$ and [Tb(**DO3A-pic-SEtCOOEt**)]$^-$, each well including the blank contains 17-18 µCi ^{177}Lu. A blank sample of [^{177}Lu][Lu(**DO3A-pic-SEtCOOEt**)]$^-$ provides a pure Cherenkov radiation sample without any luminescence contribution from Tb. Post-thioconjugation improves the QY 10-fold resulting in an increase in radiance from the "off" (NO_2) to "on" (SR_1) complexes (left). Full (uncropped) CRET plate image recorded.[**Tb(DO3A-pic-SEtCOOEt**)]$^-$ is in the first row, [**Tb(DO3A-pic-NO$_2$)**]$^-$ is in the second row, and the blank is in the third row. All wells contain 17-18 µCi [^{177}Lu][**Lu(DO3A-pic-S SEtCOOEt**)]$^-$. The concentration gradient from left to right is 50, 25, 10, 5, 2, 1, AND 0.1 nmol (right).

6. In vivo studies

All animal experiments and procedures were performed in accordance with the United States' National Institutes of Health's "Guide for the Care and Use of Laboratory Animals" and approved by Institutional Animal Care and Use Committee (IACUC) at Stony Brook Medicine under protocol number 1104609, entitled "Animal Models for the Targeted Molecular Imaging and Therapy of Cancer using Radioactive and Fluorescent Agents", expiration 7/20/2023.

PET imaging

Eight-week-old male NCru mice were inoculated subcutaneously on the right shoulder with PSMA (+) PC3 PIP cells (expression of PSMA) in 1:1 DPBS pH 7.4: Matrigel or on the left shoulder with PSMA (-) PC3 flu cells (no expression of PSMA) in 1:1 DPBS pH 7.4 : Matrigel. At day 10 post-xenograft when tumours reached a suitable size, animals were administered [^{86}Y][**Y(DO3A-pic-S-Cys-PSMA**)]$^{-}$ (10-40 µCi in DPBS) via tail-vein injection. Mice were imaged at 90 min post injection (p.i.) using Siemens Inveon PET/ CT Multimodality System, and image analysis was conducted using AMIDE.

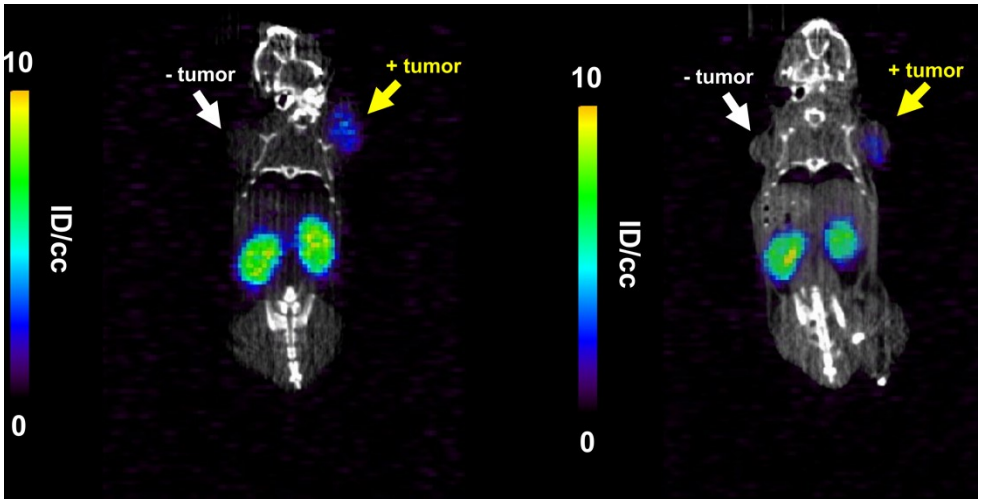

Figure S17: PET scan (top view) of mice injected with [^{86}Y][**Y(DO3A-pic-S-Cys-PSMA**)]$^{-}$ 90 min post-injection. The PSMA positive tumours are indicated with an arrow.

Biodistribution

The 10 male NCru athymic nude mice were anesthetized with isoflurane, and 12-18 µCi of [^{86}Y][**Y(DO3A-pic-NO$_2$)**]$^-$ or 10-40 µCi of [^{86}Y][**Y(DO3A-pic-S-Cys-PSMA**)]$^-$ was intravenously injected via tail-vein catheter. Mice were sacrificed at 2 h post-injection, and select organs were harvested. Radioactivity was counted by using a gamma counter, and the radioactivity associated with each organ was expressed as %ID/g. Biodistribution data were assessed by unpaired t tests using GraphPad Prism to determine if differences between groups were statistically significant ($p < 0.05$).

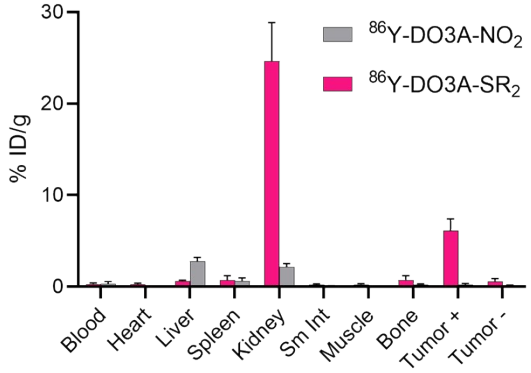

Figure S18: Bar chart of 2 h biodistribution of [^{86}Y][**Y(DO3A-pic-SR$_2$)**]$^-$ (n = 5) and [^{86}Y][**Y(DO3A-pic-NO$_2$)**]$^-$ (n = 5).

Table S3: Numerical values of 2 h biodistribution of [^{86}Y][**Y(DO3A-pic-SR$_2$)**]$^-$ (n = 5).

	[^{86}Y][**Y(DO3A-pic-SR$_2$)**]$^-$						
[%ID/g]	Mouse 1	Mouse 2	Mouse 3	Mouse 4	Mouse 5	Mean	Std. dev.
Blood	0.22	0.24	0.53	0.17	0.23	0.278	0.143
Heart	0.18	0.22	0.50	0.18	0.22	0.260	0.136
Liver	0.63	0.55	0.72	0.66	0.46	0.604	0.101
Spleen	0.50	0.35	1.59	0.48	0.68	0.720	0.500
Kidney	23.04	22.14	31.71	25.20	21.08	24.634	4.236
Small Intestine	0.15	0.13	0.41	0.16	0.16	0.202	0.117
Muscle	0.24	0.17	0.42	0.14	0.22	0.238	0.109
Bone	0.53	0.41	1.53	0.42	0.79	0.736	0.470
Tumor +	6.95	7.19	4.73	7.05	4.63	6.110	1.309
Tumor -	0.57	1.07	0.62	0.27	0.23	0.552	0.338

Table S4: Numerical values of 2 h biodistribution of [^{86}Y][**Y(DO3A-pic-NO$_2$)**]$^-$ (n = 5).

	[^{86}Y][**Y(DO3A-pic-NO$_2$)**]$^-$						
[%ID/g]	Mouse 6	Mouse 7	Mouse 8	Mouse 9	Mouse 10	Mean	Std. dev.
Blood	0.11	0.62	0.56	0.13	0.13	0.310	0.257
Heart	0.08	0.08	0.09	0.09	0.07	0.082	0.008
Liver	2.90	2.61	2.98	2.19	3.30	2.796	0.418
Spleen	0.24	0.76	1.04	0.80	0.33	0.634	0.338
Kidney	2.28	1.71	2.19	1.96	2.72	2.172	0.378
Small Intestine	0.05	0.06	0.06	0.10	0.11	0.076	0.027
Muscle	0.03	0.06	0.07	0.06	0.06	0.056	0.015
Bone	0.16	0.26	0.27	0.23	0.32	0.248	0.059
Tumor +	0.16	0.37	0.36	0.00	0.15	0.208	0.157
Tumor -	0.15	0.17	0.14	0.21	0.15	0.164	0.028

Metabloite analysis

Urine was collected from mice 1, 5 (both injected with [^{86}Y][**Y(DO3A-pic-S-Cys-PSMA**)]$^{-}$), and 7 (injected with [^{86}Y][**Y(DO3A-pic-NO$_2$)**]$^{-}$). The other animals did not have a sufficient quantity of urine. The collected urine was injected into an HPLC and fractions were collected for every 30 s. Radioactivity of measured with a gamma counter. Differences in the retention time of peaks are attributed to the severely decreased resolution of collecting fractions at 30 s intervals versus online detection on the HPLC- as well as the time difference between radiodetector and outlet for collection.

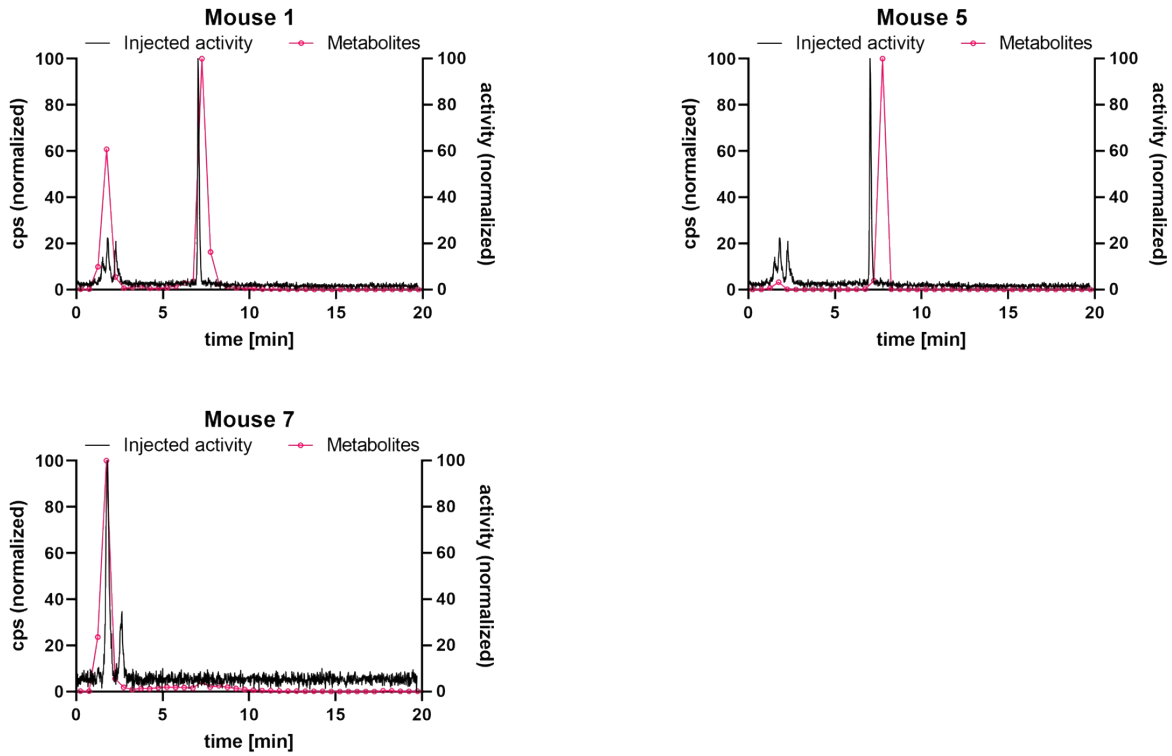

Figure S19: Metabolite analysis of the urine collected from 3 mice, showing the HPLC γ-trace of the injected compounds versus the activity measured from collected HPLC urine samples 2 h post-injection. Mice 1 & 5 were injected with [^{86}Y][**Y(DO3A-pic-SCys-PSMA**)]$^{-}$, mouse 7 was injected with [^{86}Y][**Y(DO3A-pic-NO$_2$)**]$^{-}$.

7. Spectra

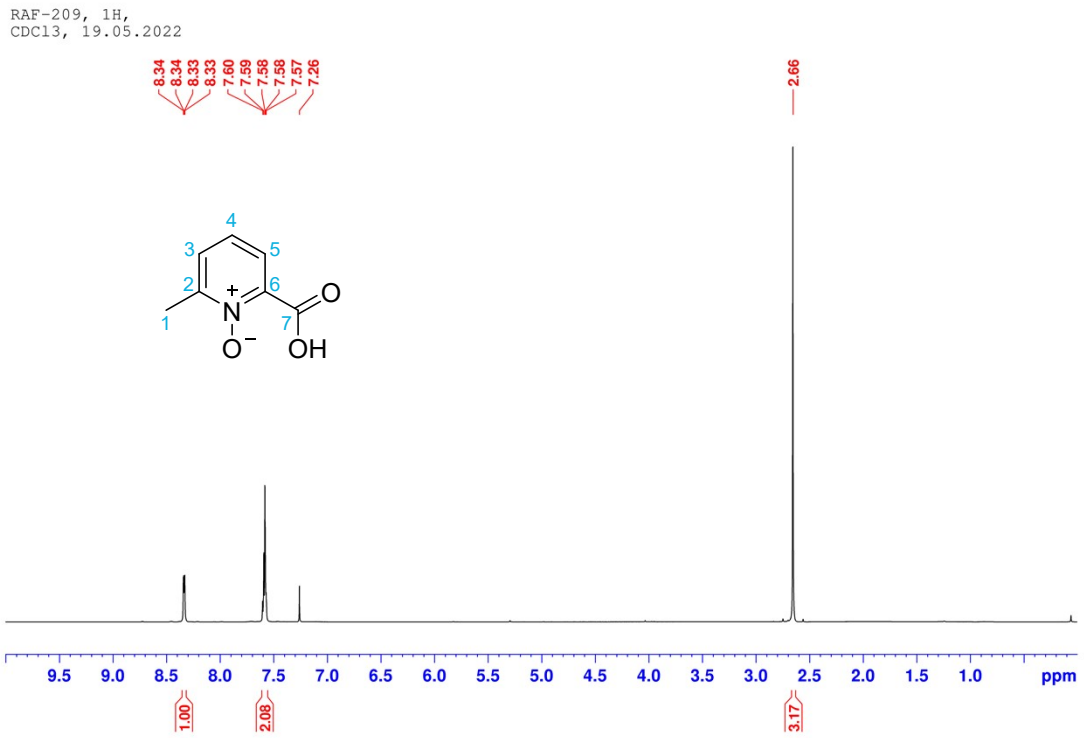

Figure S20: ^{1}H NMR of **S1**.

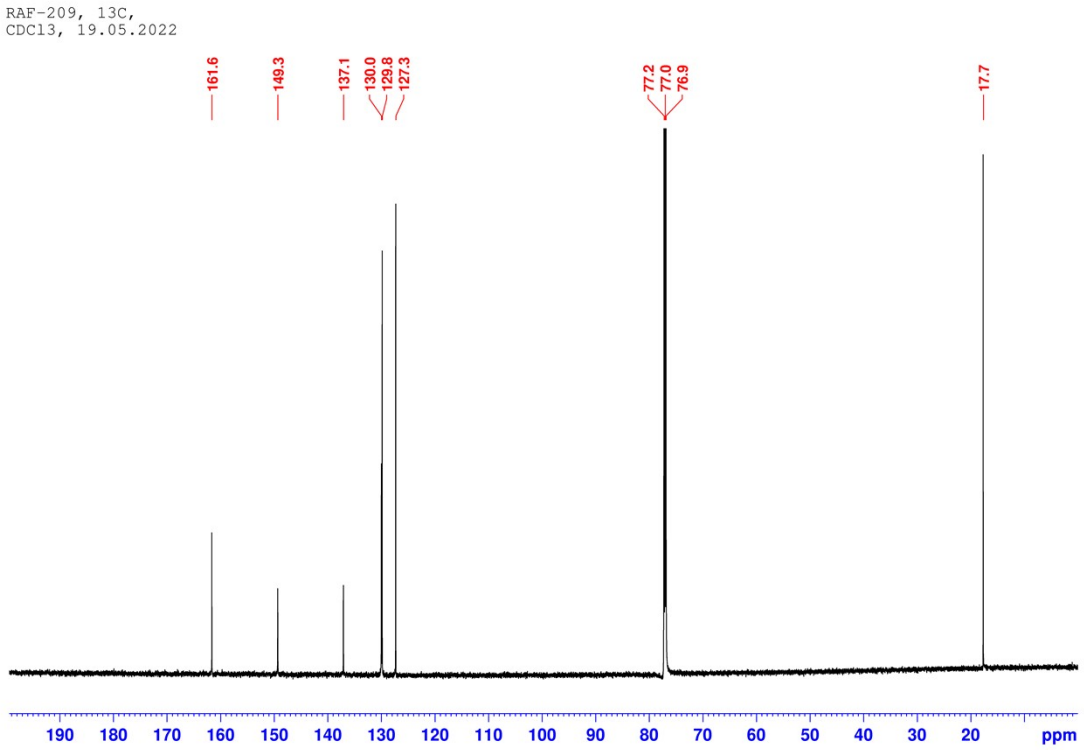

Figure S21: ^{13}C NMR of **S1**.

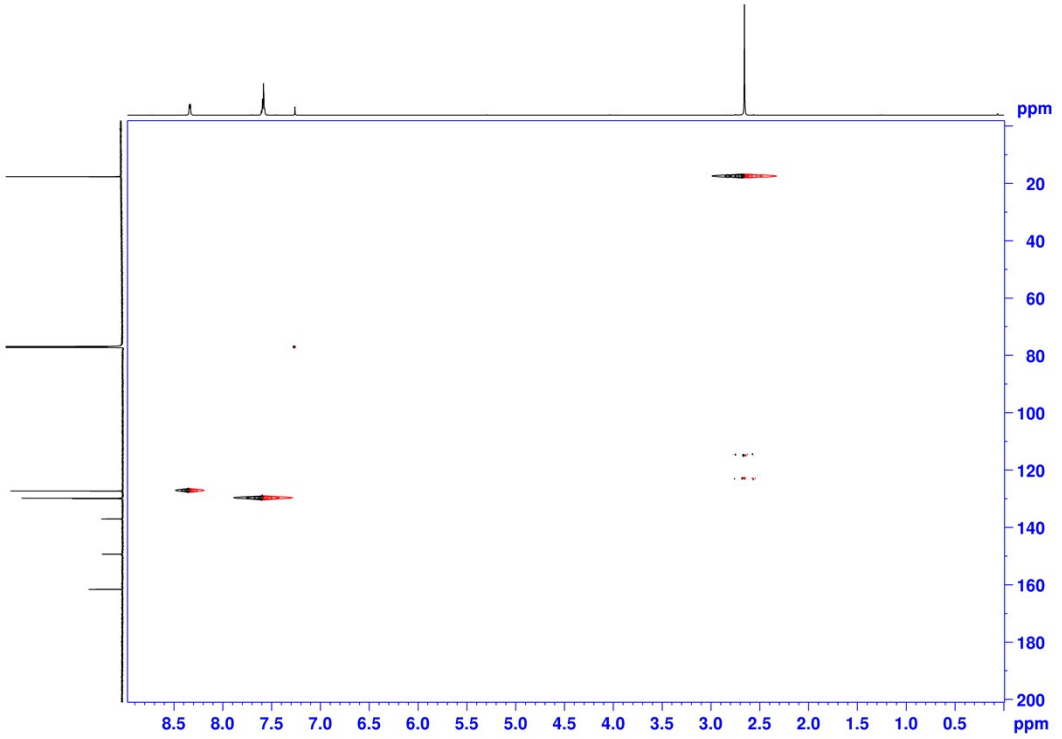

Figure S22: HSQC of **S1**.

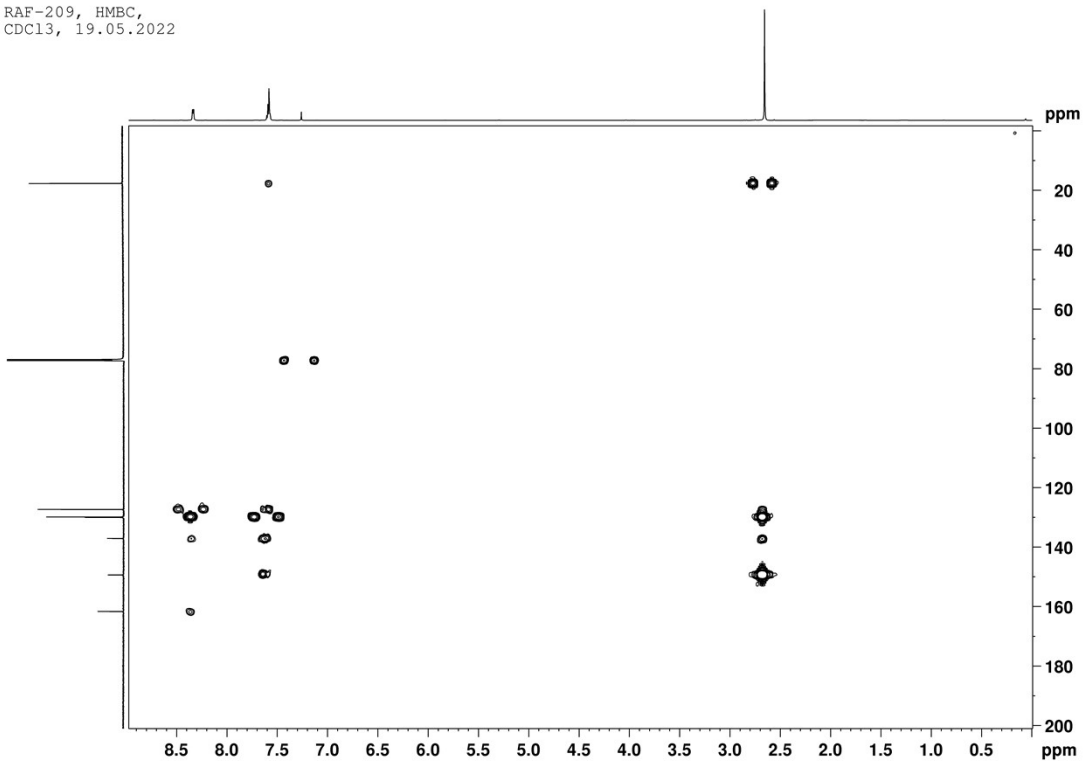

Figure S23: HMBC of **S1**.

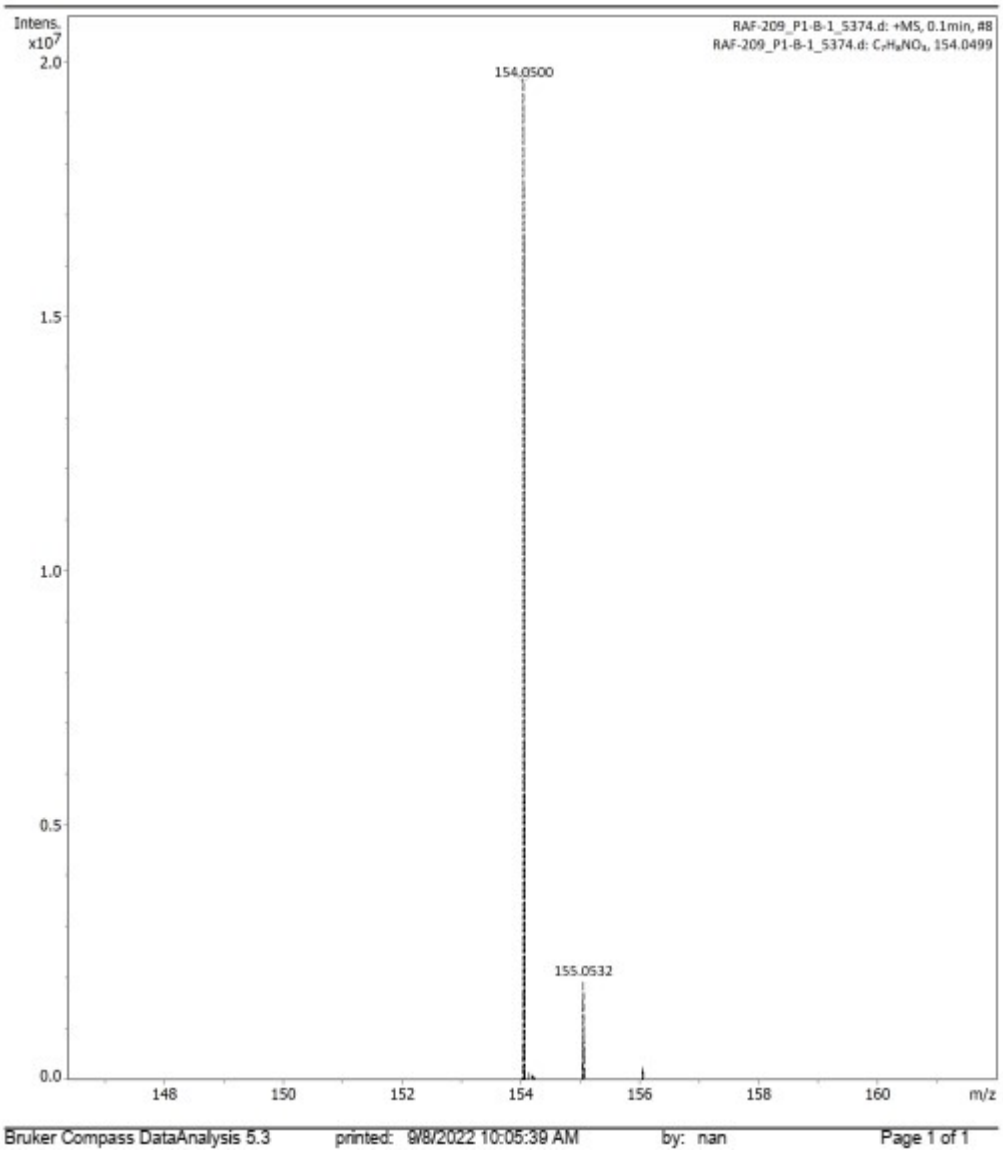

Figure S24: HR-ESI-MS of **S1**.

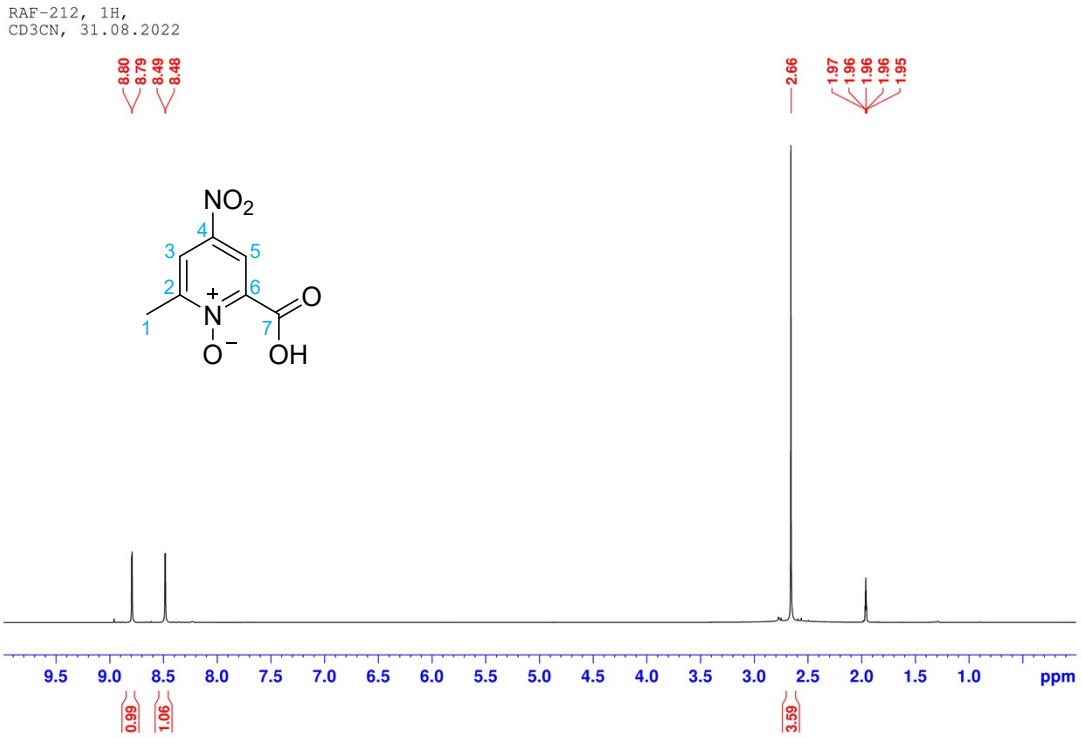

Figure S25: ^{1}H NMR of **S2**.

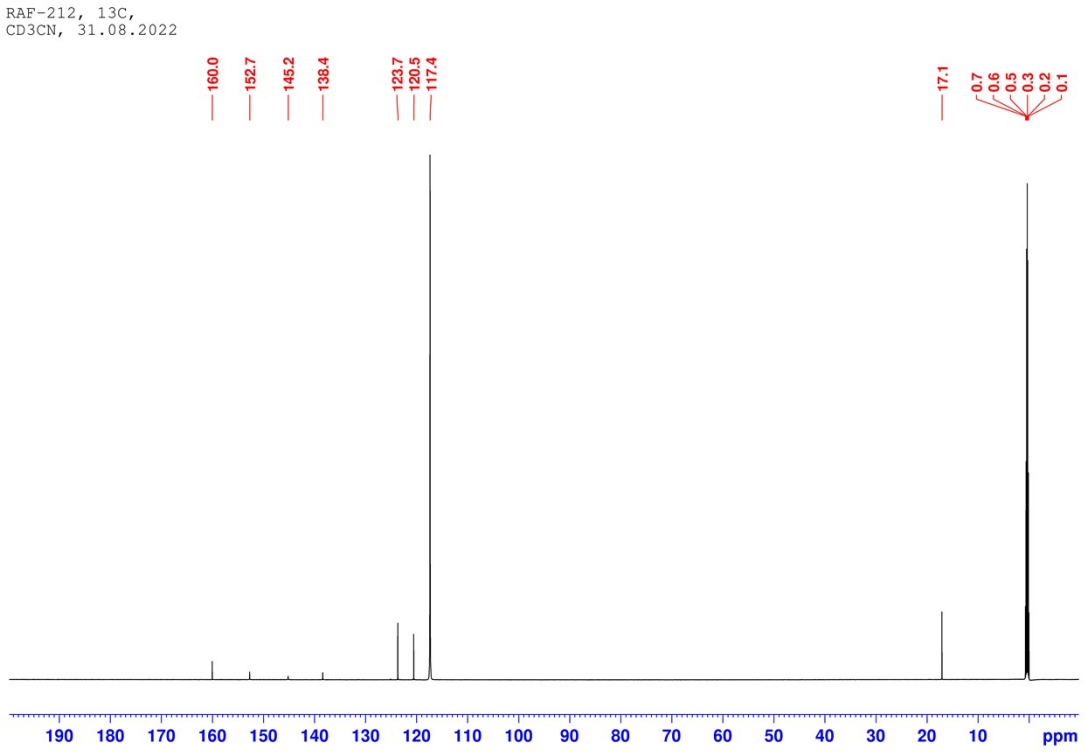

Figure S26: ^{13}C NMR of **S2**.

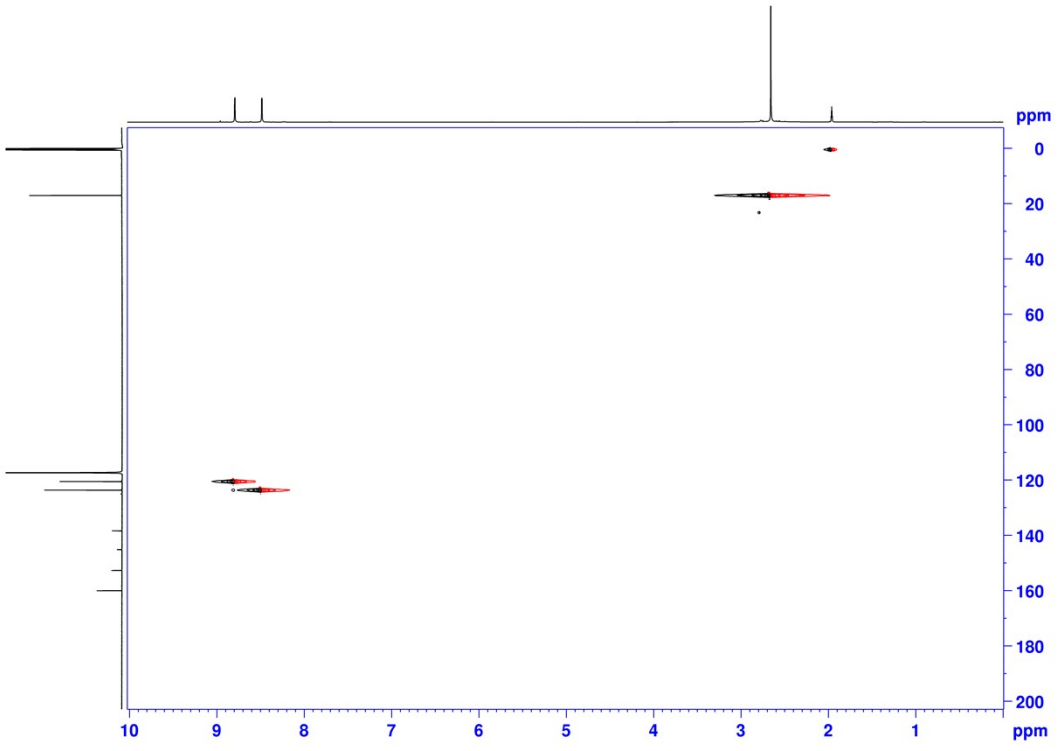

Figure S27: HSQC of **S2**.

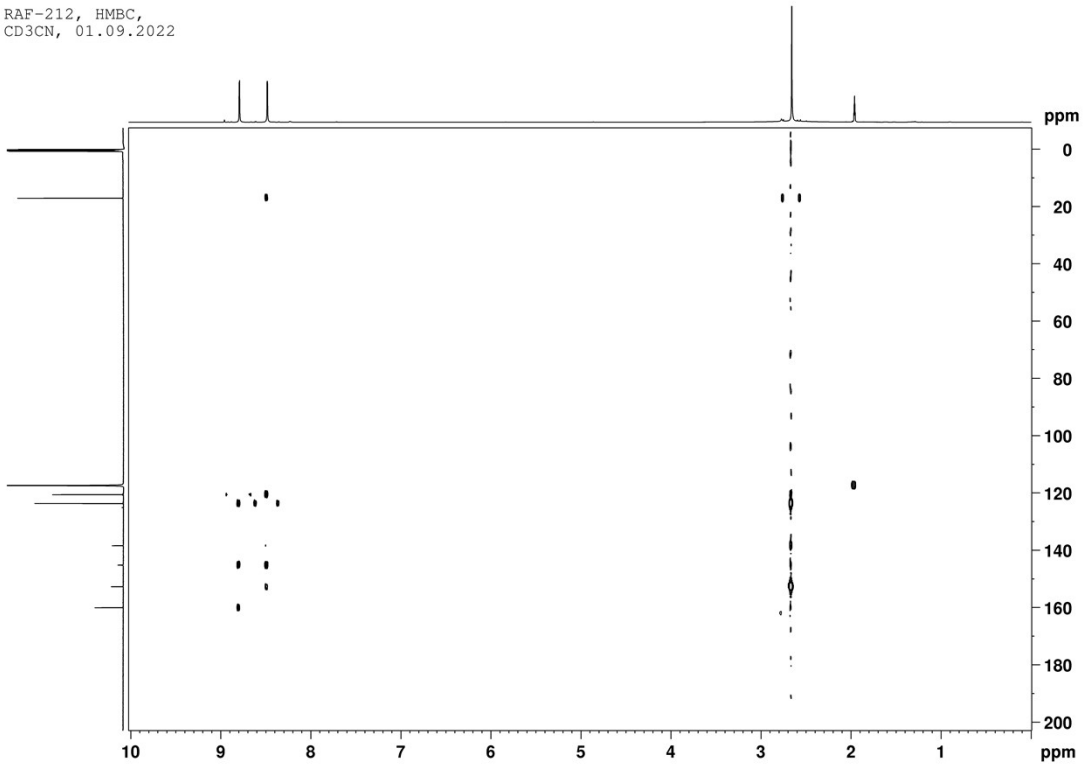

Figure S28: HMBC of **S2**.

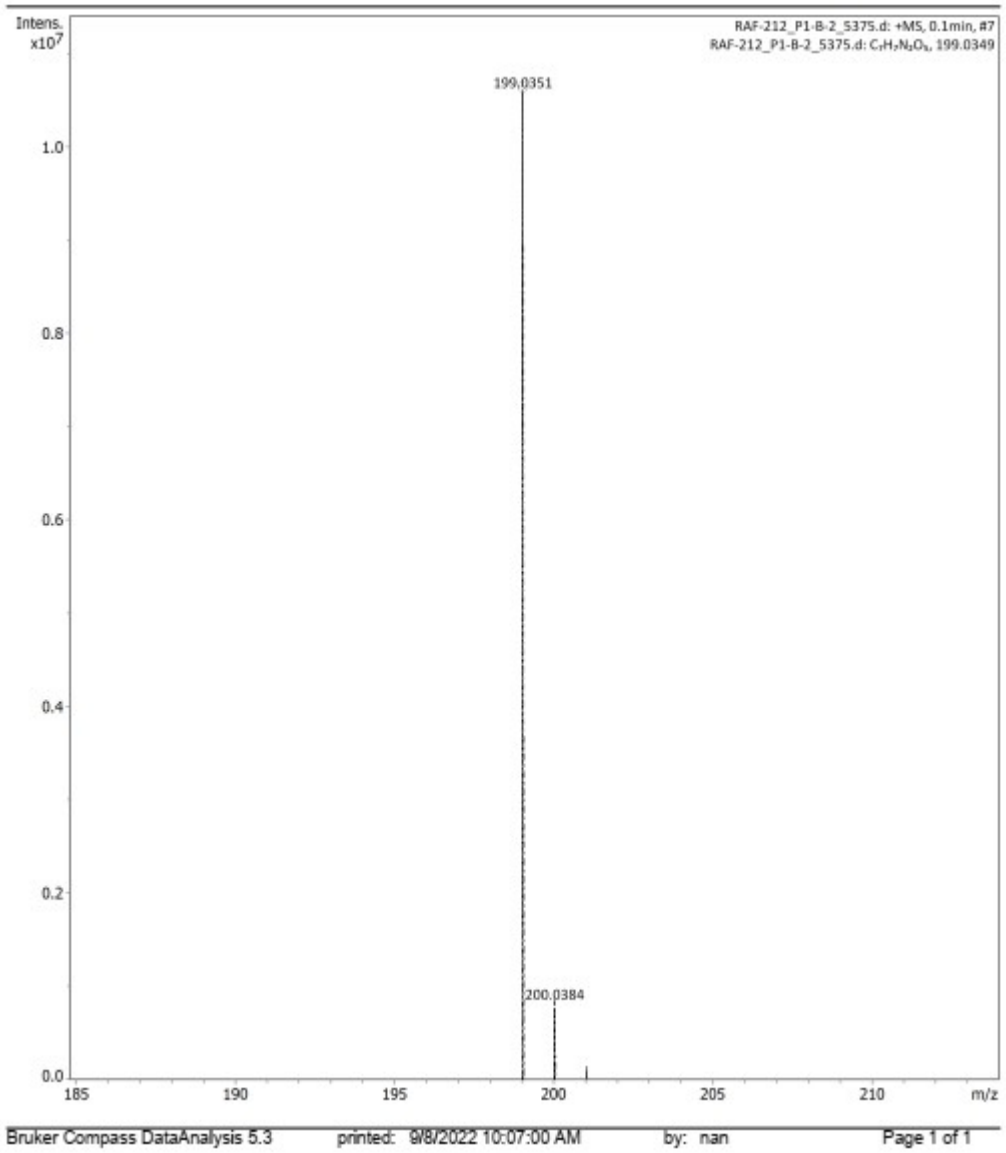

Figure S29: HR-ESI-MS of **S2**.

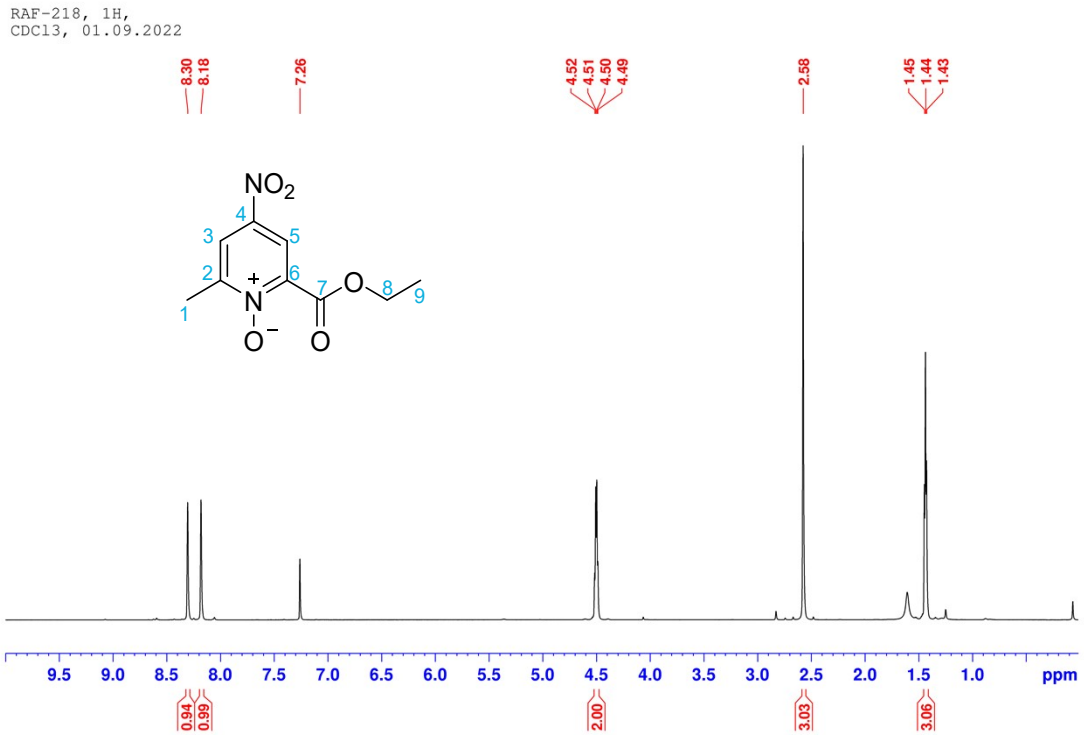

Figure S30: ^{1}H NMR of **S3**.

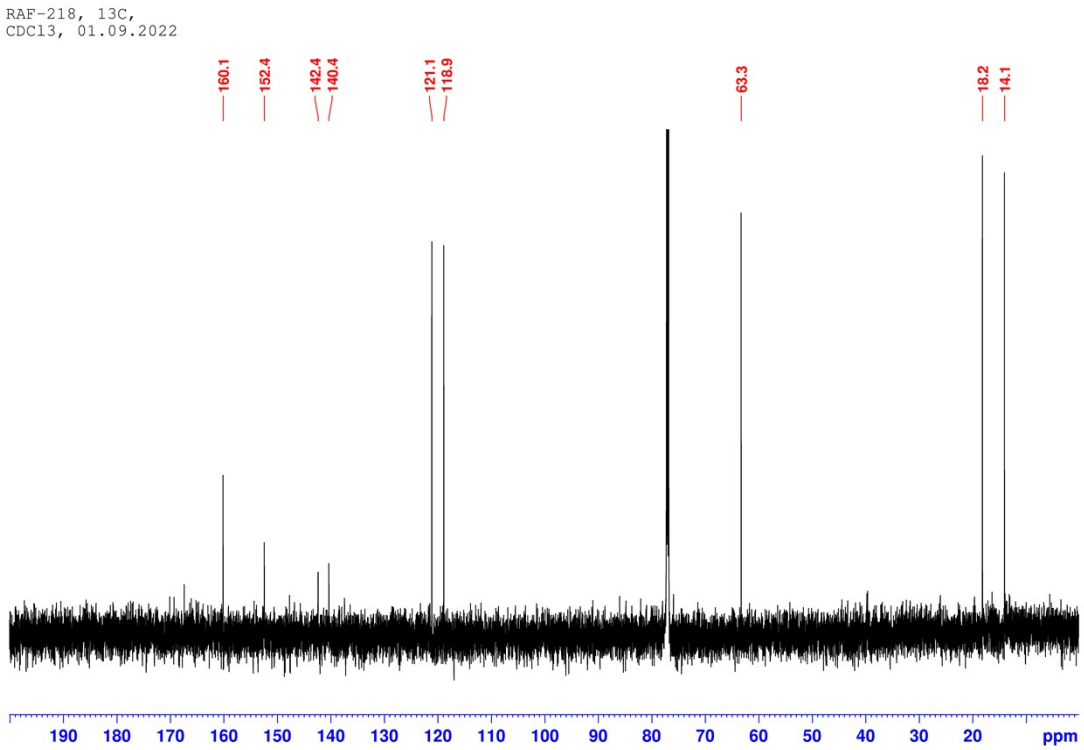

Figure S31: ^{13}C NMR of **S3**.

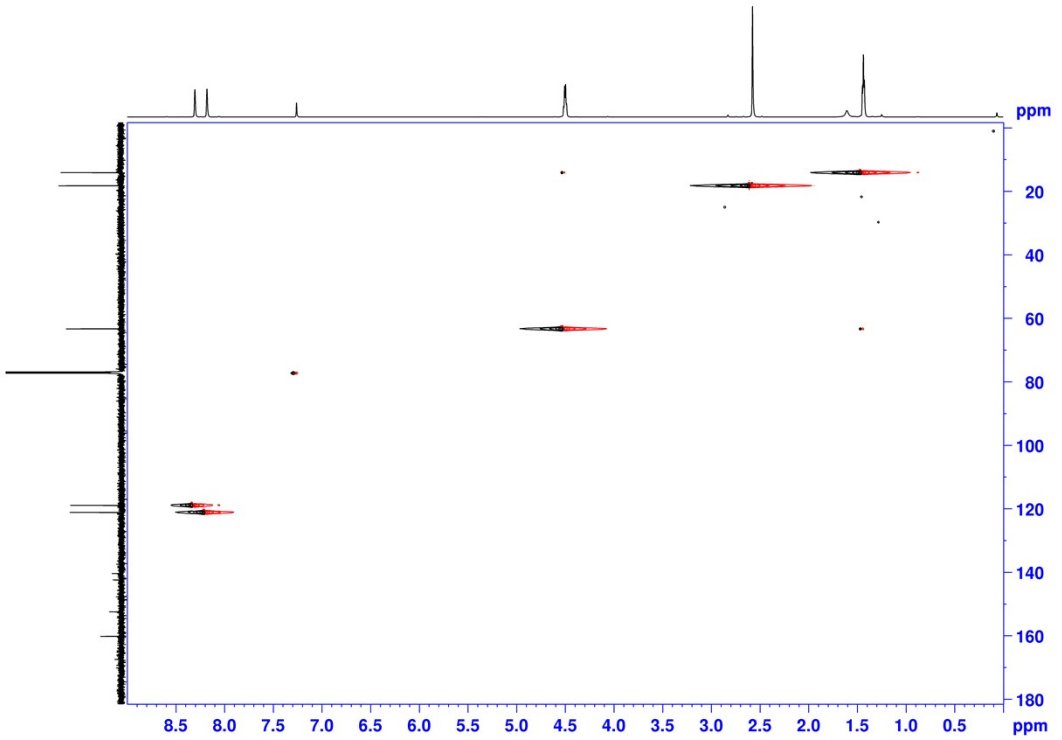

Figure S32: HSQC of **S3**.

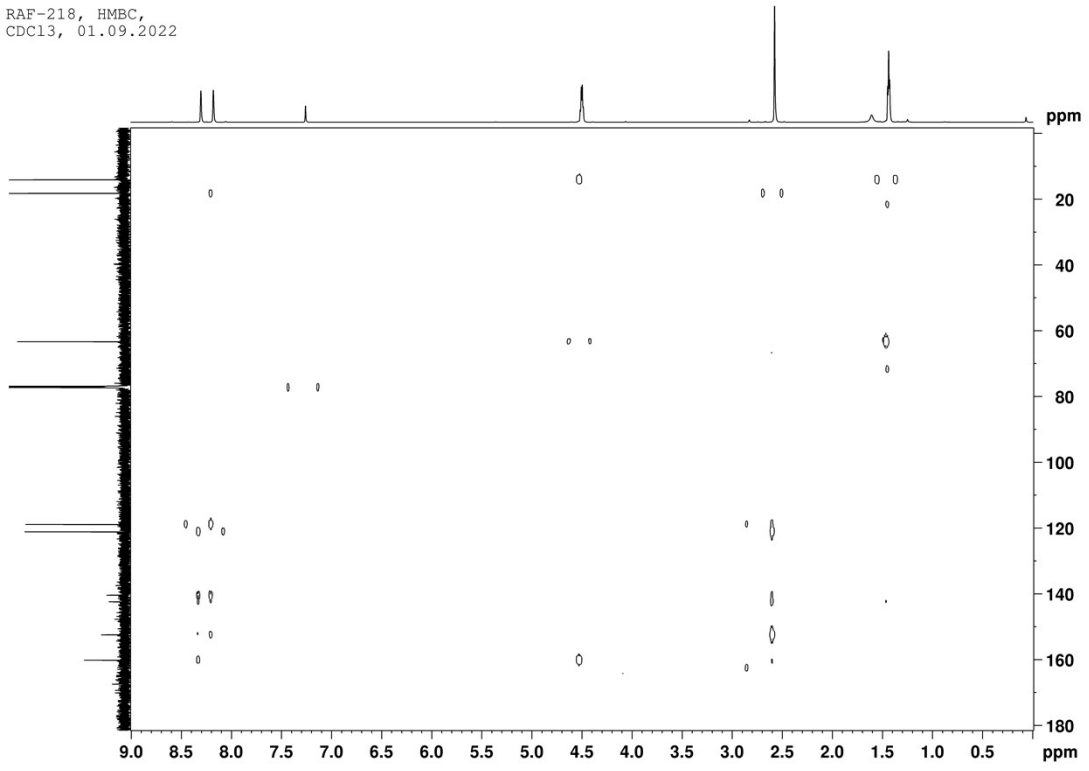

Figure S33: HMBC of **S3**.

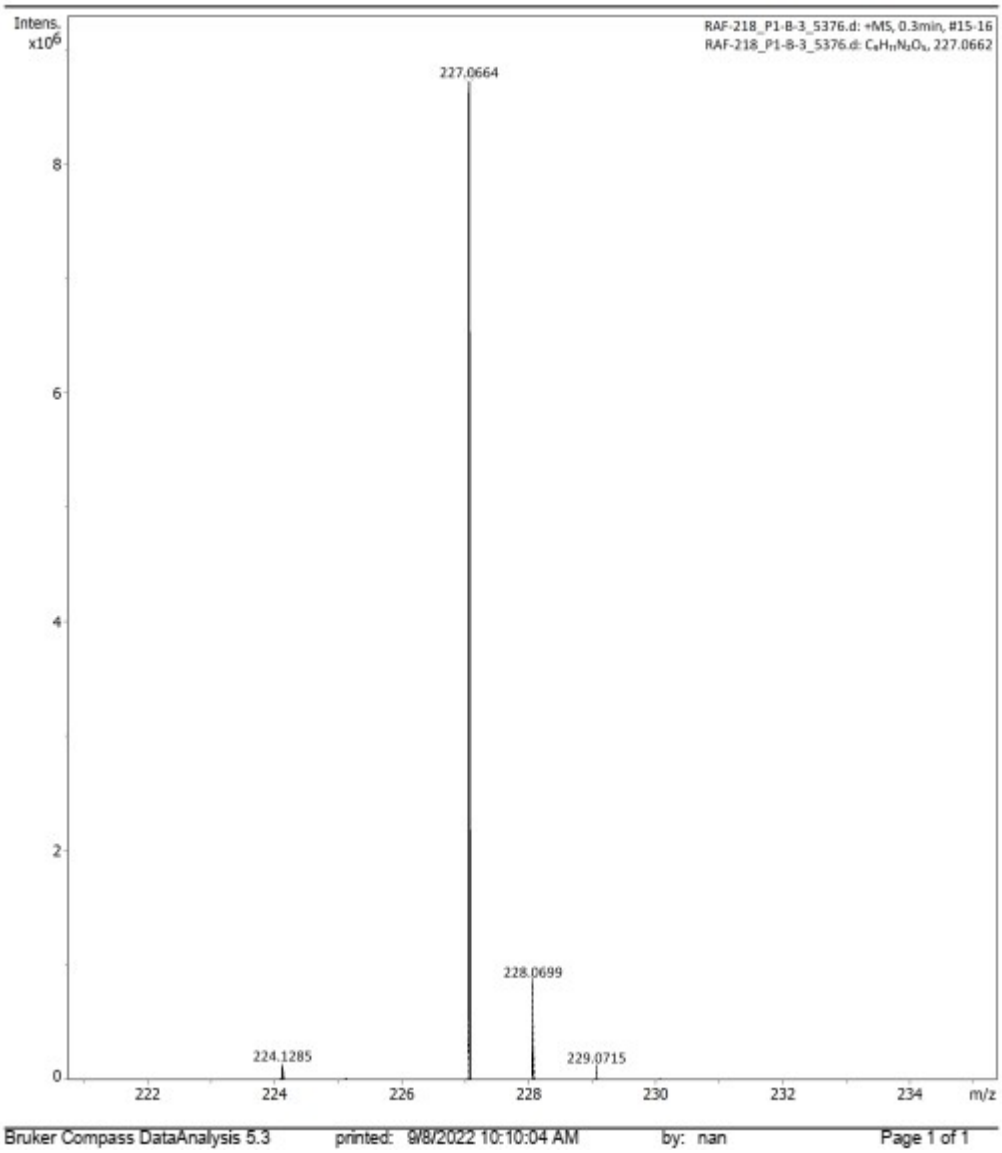

Figure S34: HR-ESI-MS of **S3**.

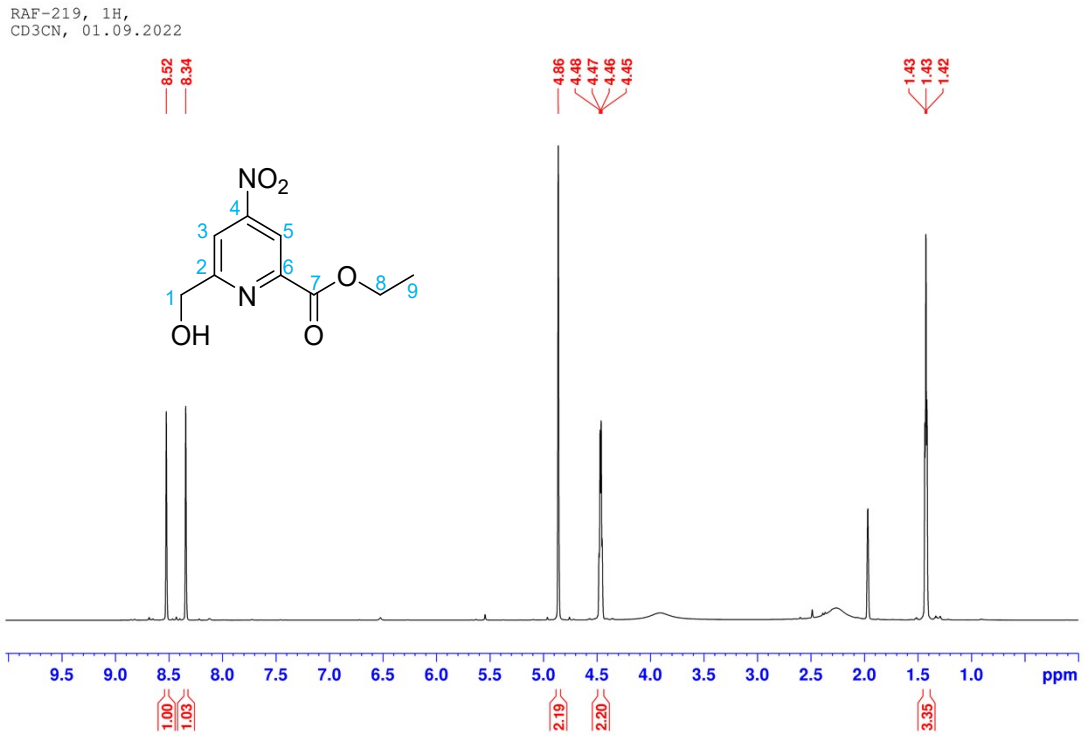

Figure S35: ^{1}H NMR of **S4**.

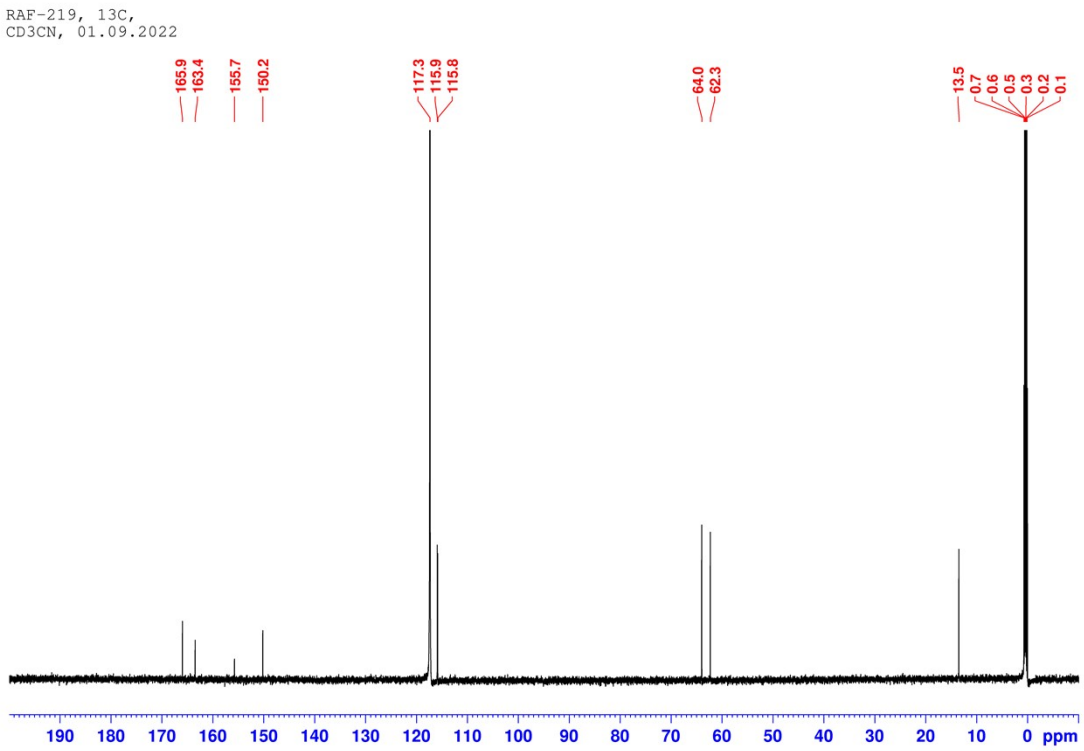

Figure S36: ^{13}C NMR of **S4**.

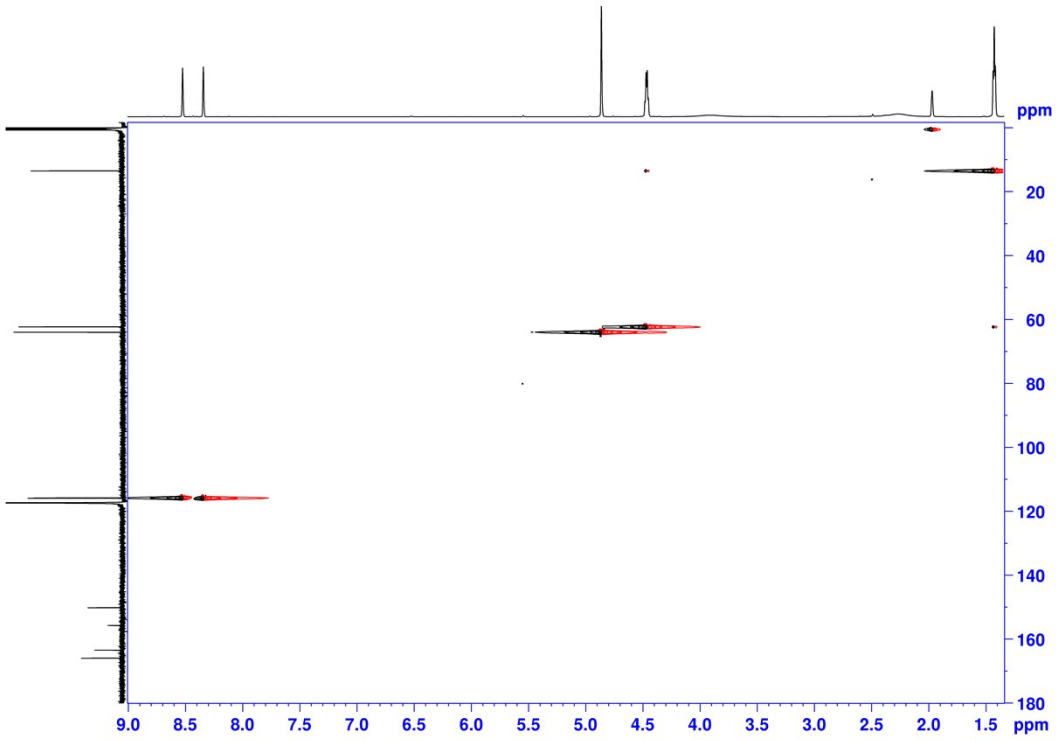

Figure S37: HSQC of **S4**.

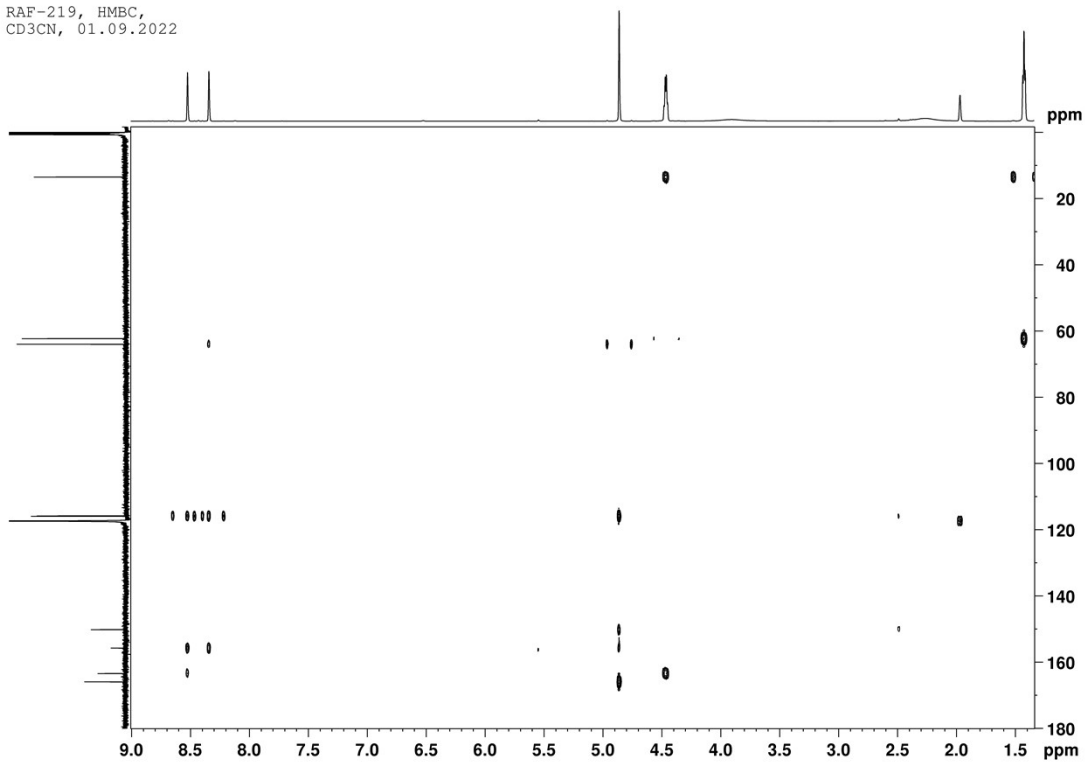

Figure S38: HMBC of **S4**.

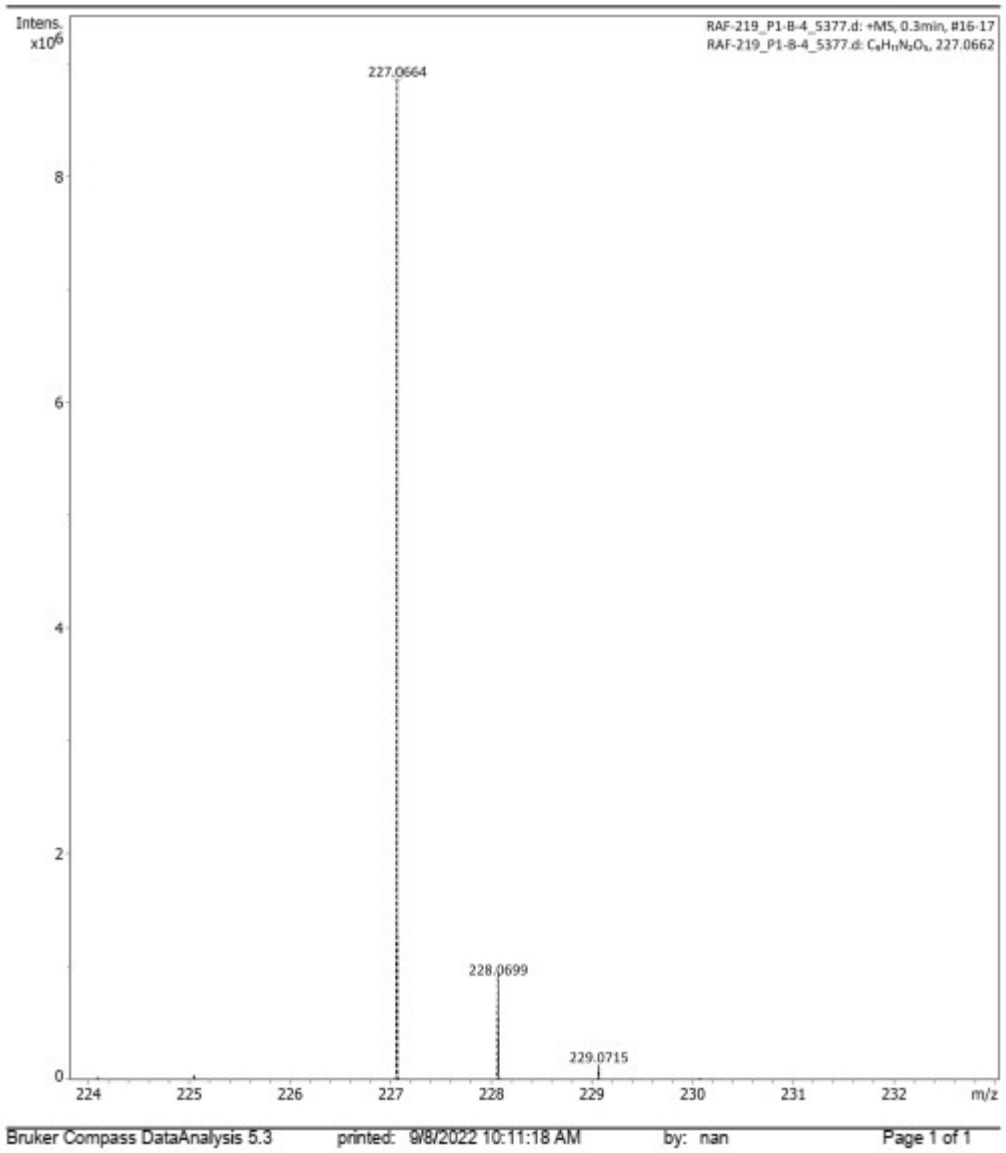

Figure S39: HR-ESI-MS of **S4**.

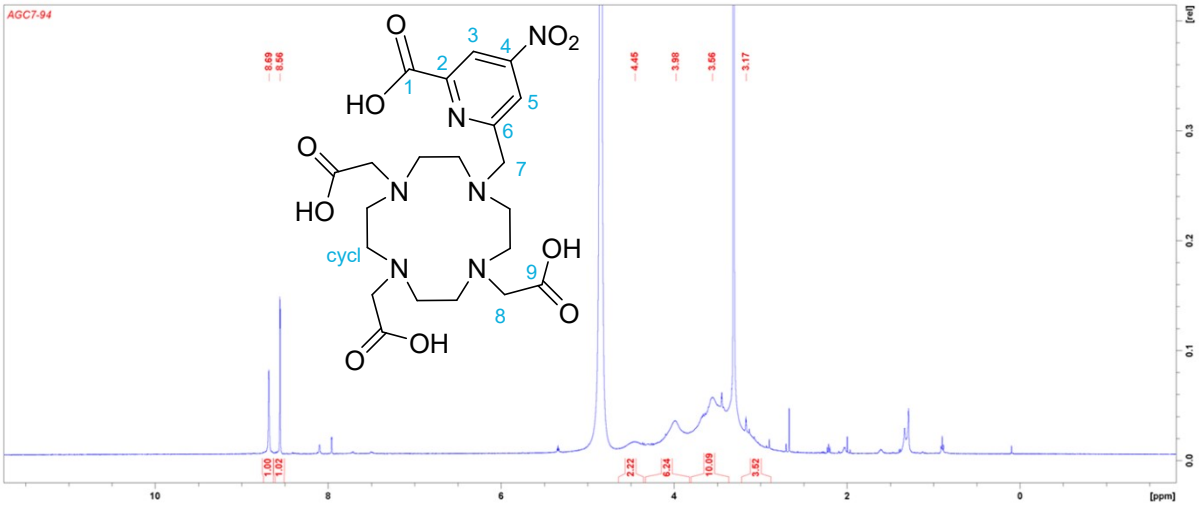

Figure S40: ^{1}H NMR of **DO3Apic-NO$_2$**.

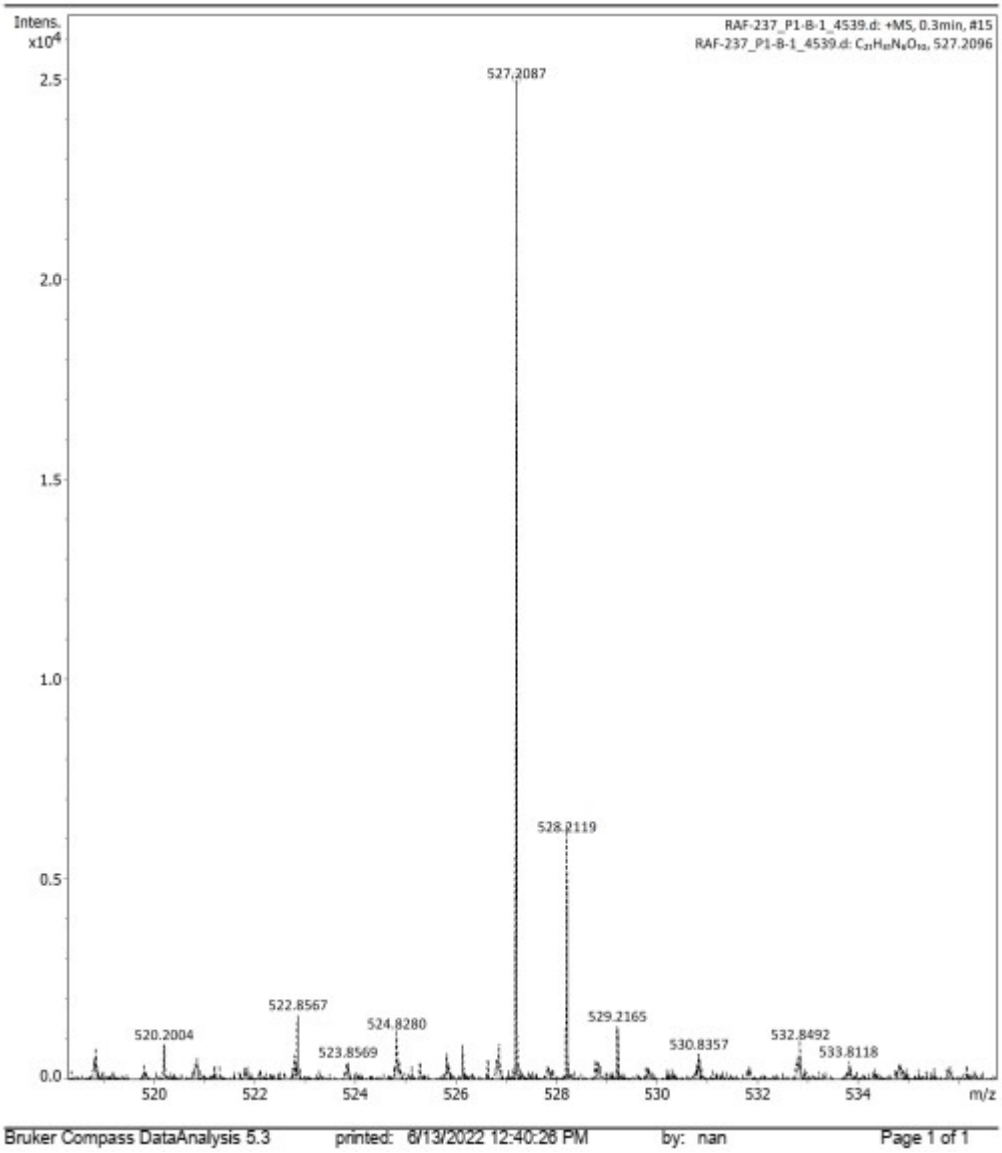

Figure S41: HR-ESI-MS of **DO3Apic-NO$_2$**.

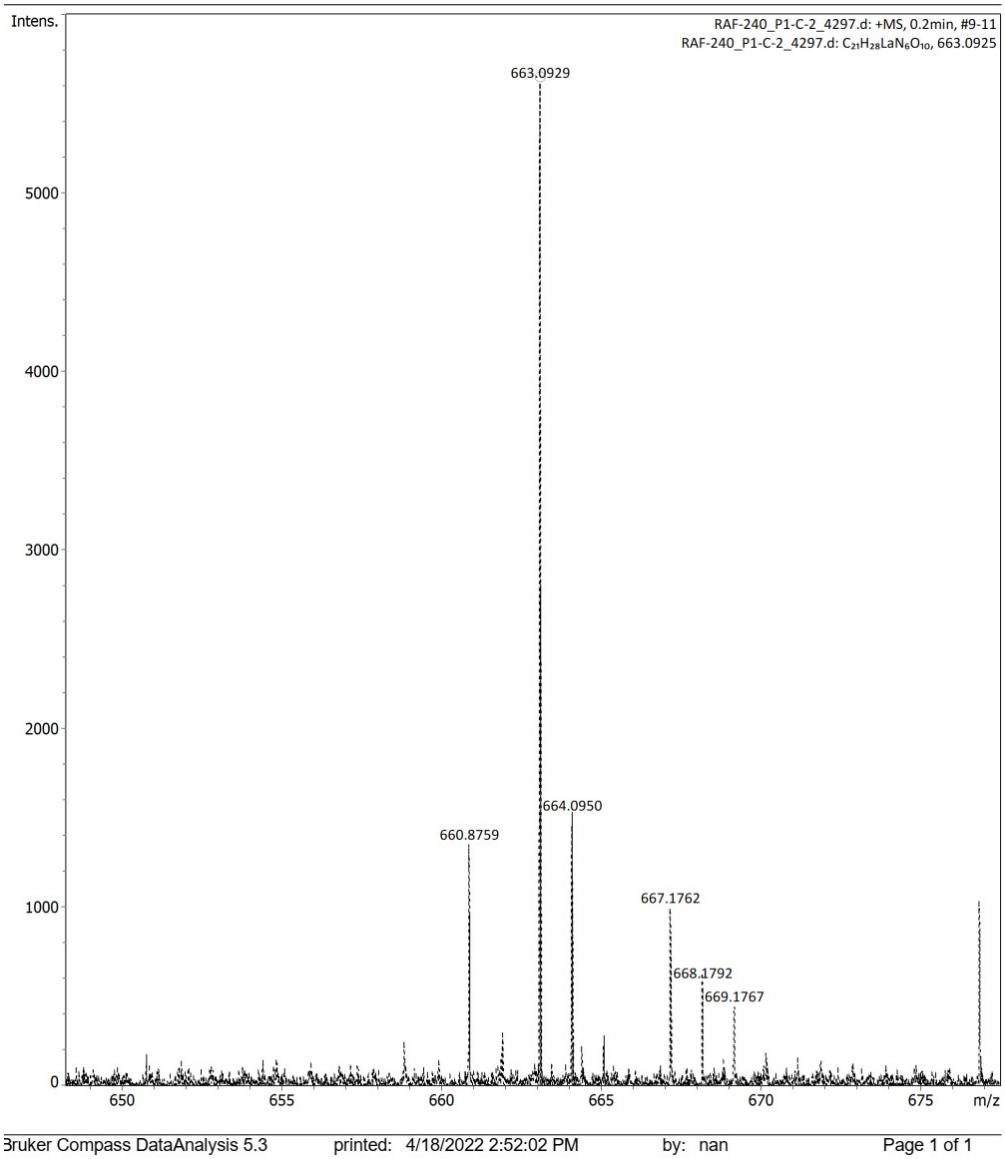

Figure S42: HR-ESI-MS of **[La(DO3Apic-NO_2)]**$^-$.

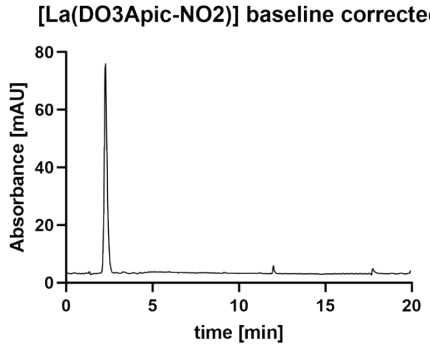

Figure S43: HPLC of **[La(DO3Apic-NO_2)]**$^-$.

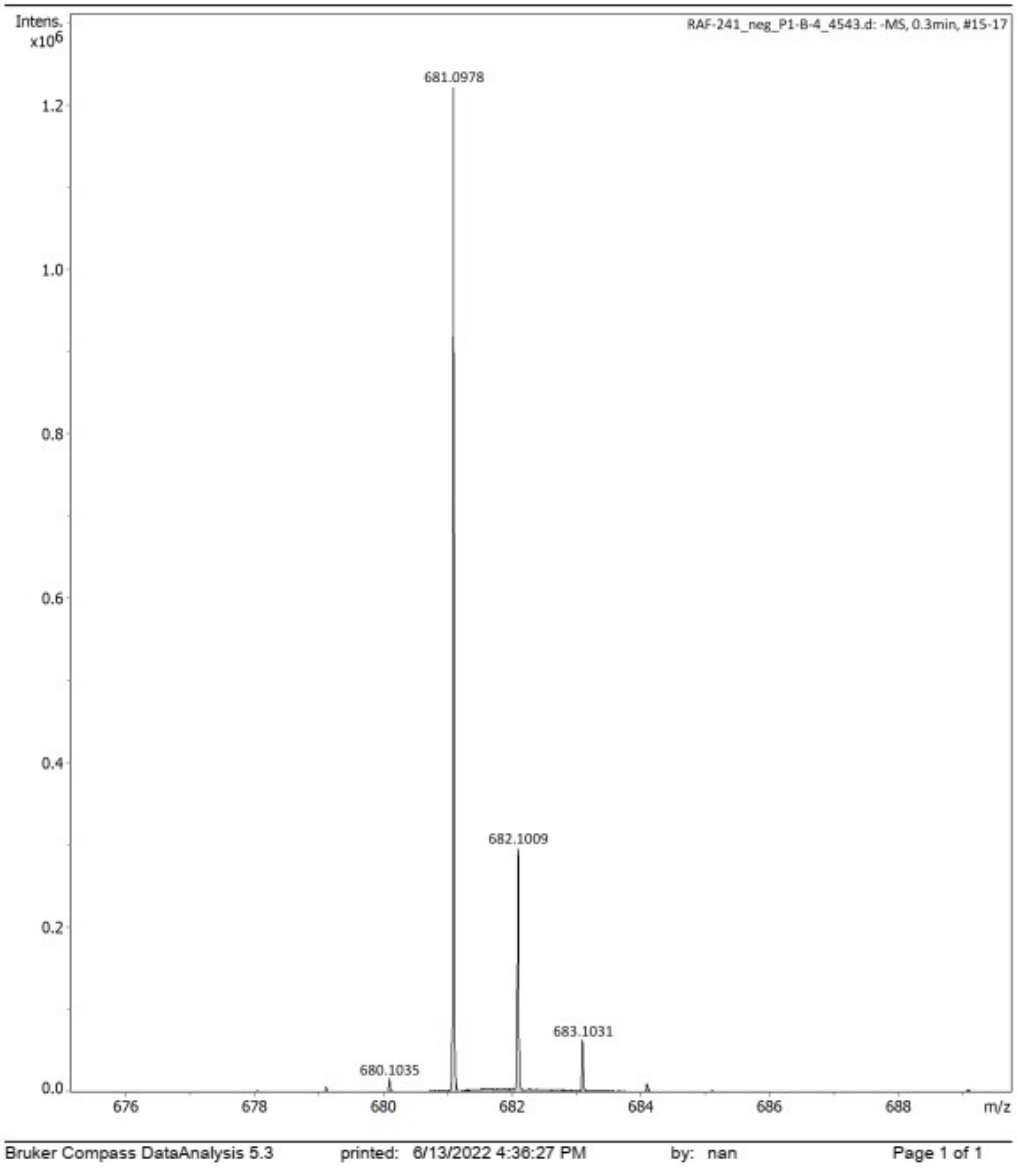

Figure S44: HR-ESI-MS of **[Tb(DO3Apic-NO$_2$)]**$^-$.

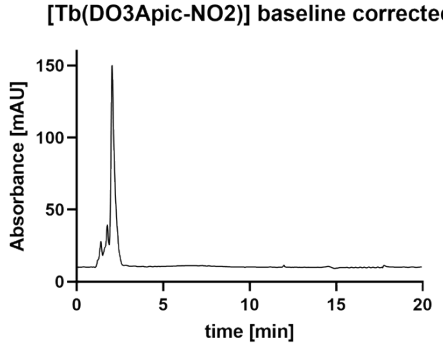

Figure S45: HPLC of **[Tb(DO3Apic-NO$_2$)]**$^-$.

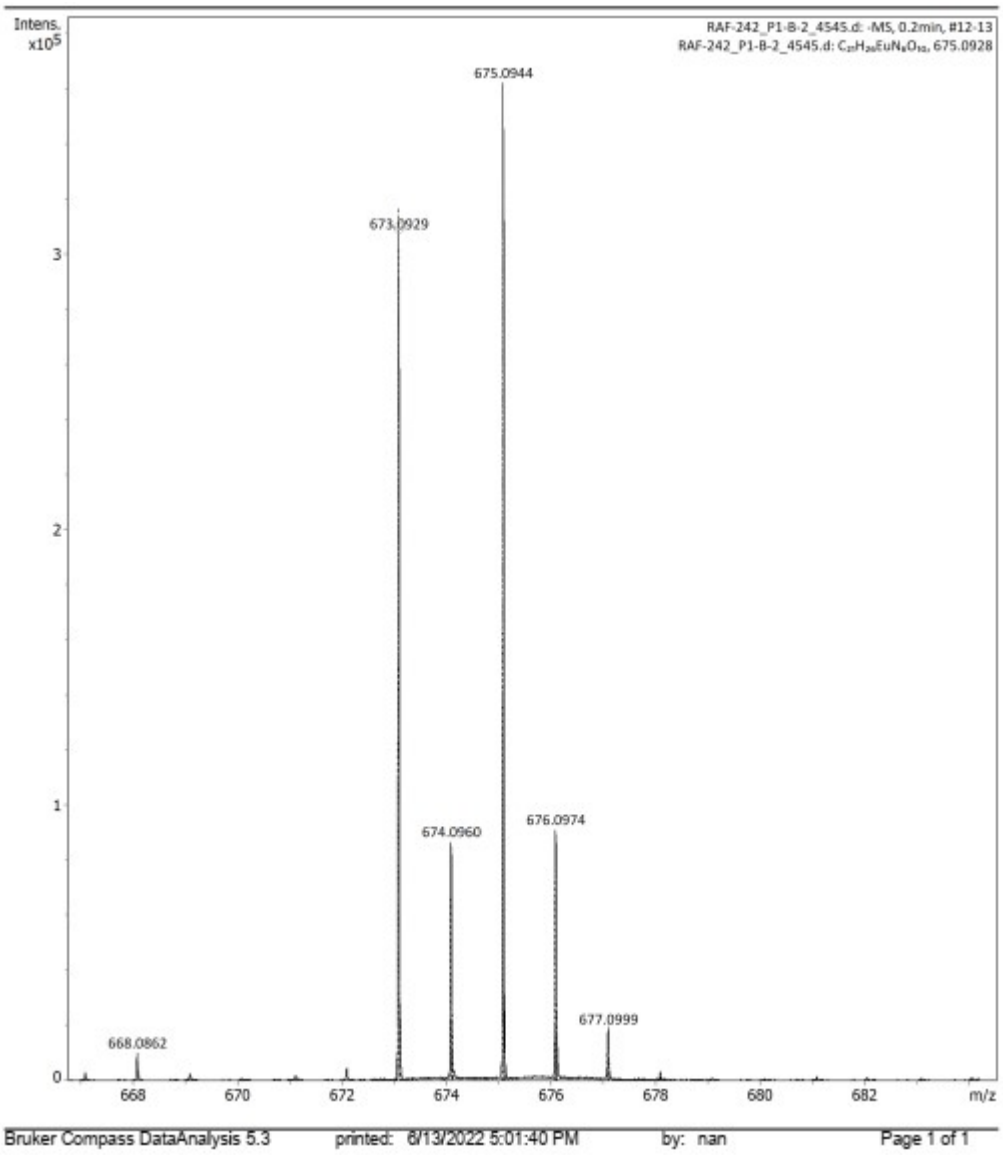

Figure S46: HR-ESI-MS of **[Eu(DO3Apic-NO$_2$)]**$^-$.

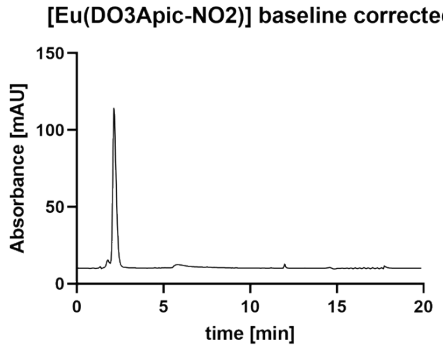

Figure S47: HPLC of **[Eu(DO3Apic-NO$_2$)]**$^-$.

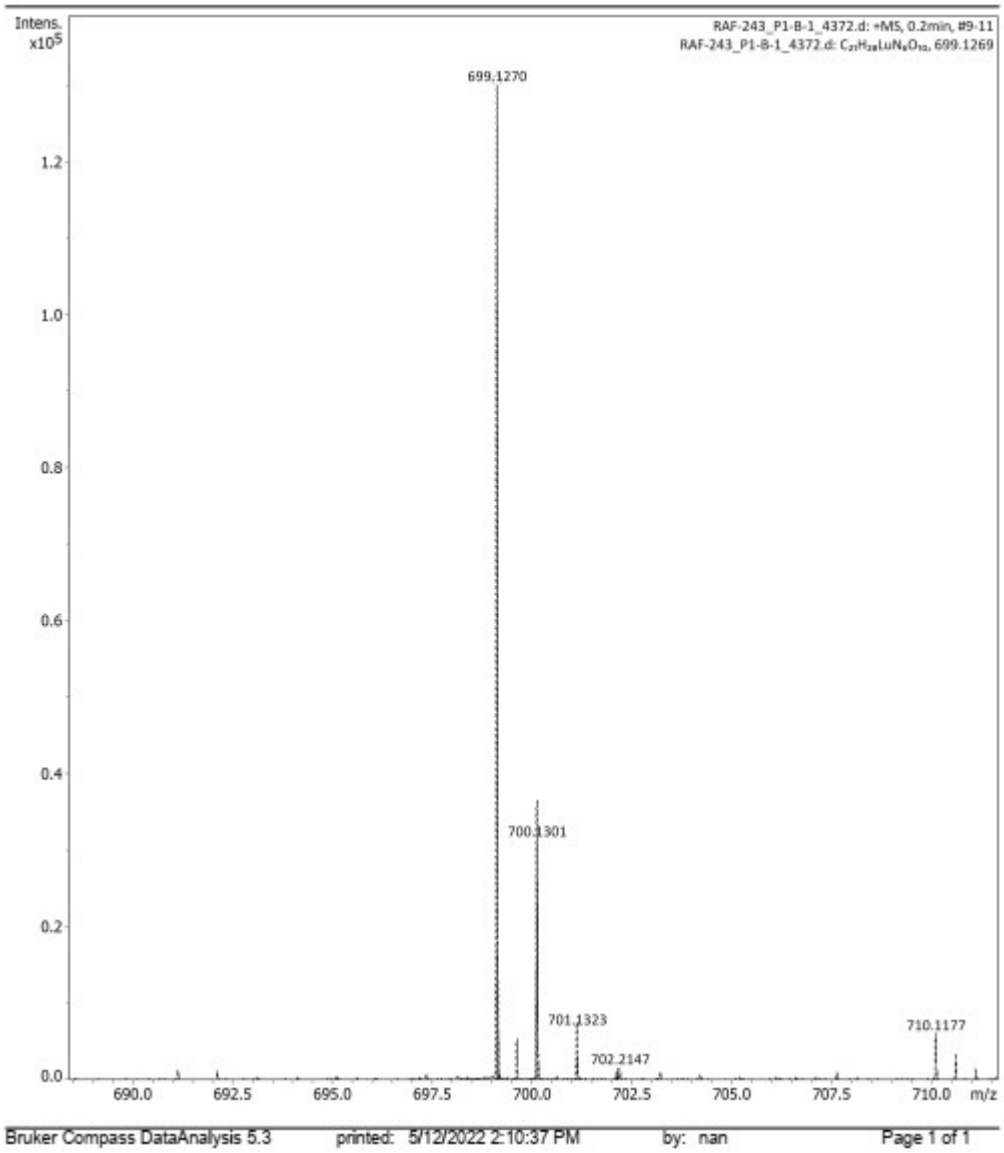

Figure S48: HR-ESI-MS of **[Lu(DO3Apic-NO_2)]**$^-$.

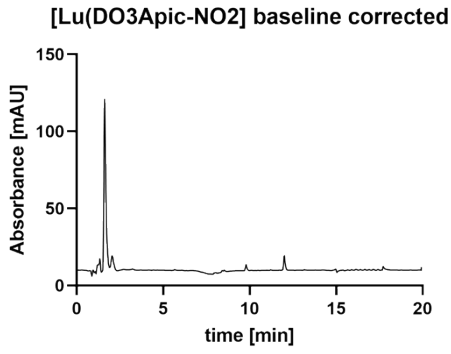

Figure S49: HPLC of **[Lu(DO3Apic-NO_2)]**$^-$.

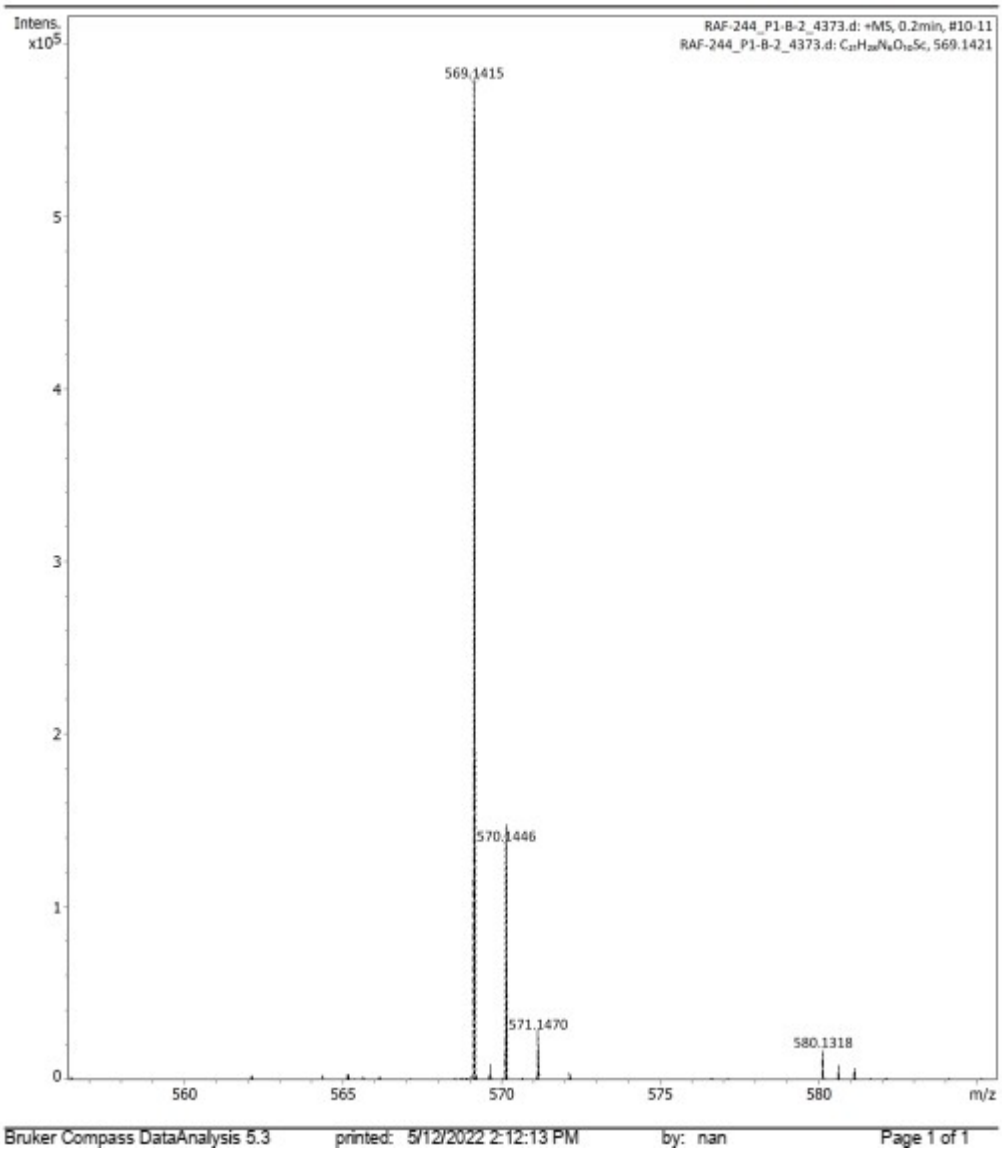

Figure S50: HR-ESI-MS of **[Sc(DO3Apic-NO_2)]**$^-$.

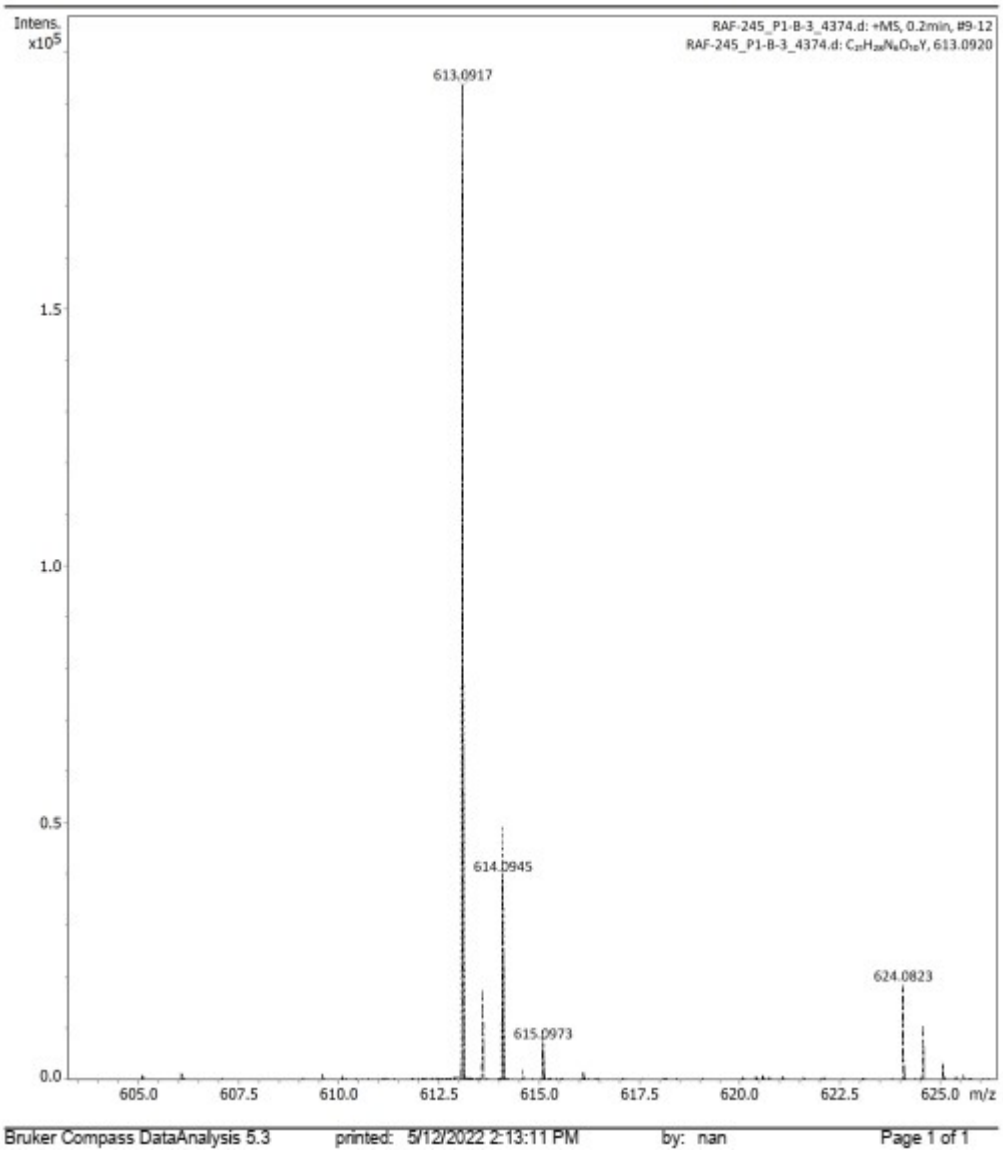

Figure S51: HR-ESI-MS of **[Y(DO3Apic-NO$_2$)]**$^-$.

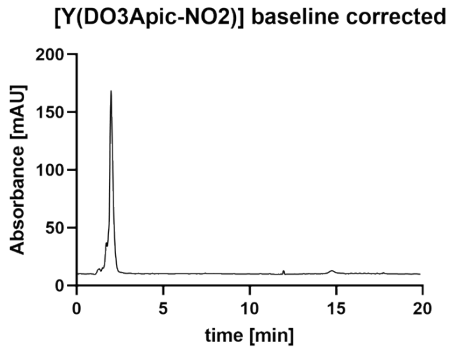

Figure S52: HPLC of **[Y(DO3Apic-NO$_2$)]**$^-$.

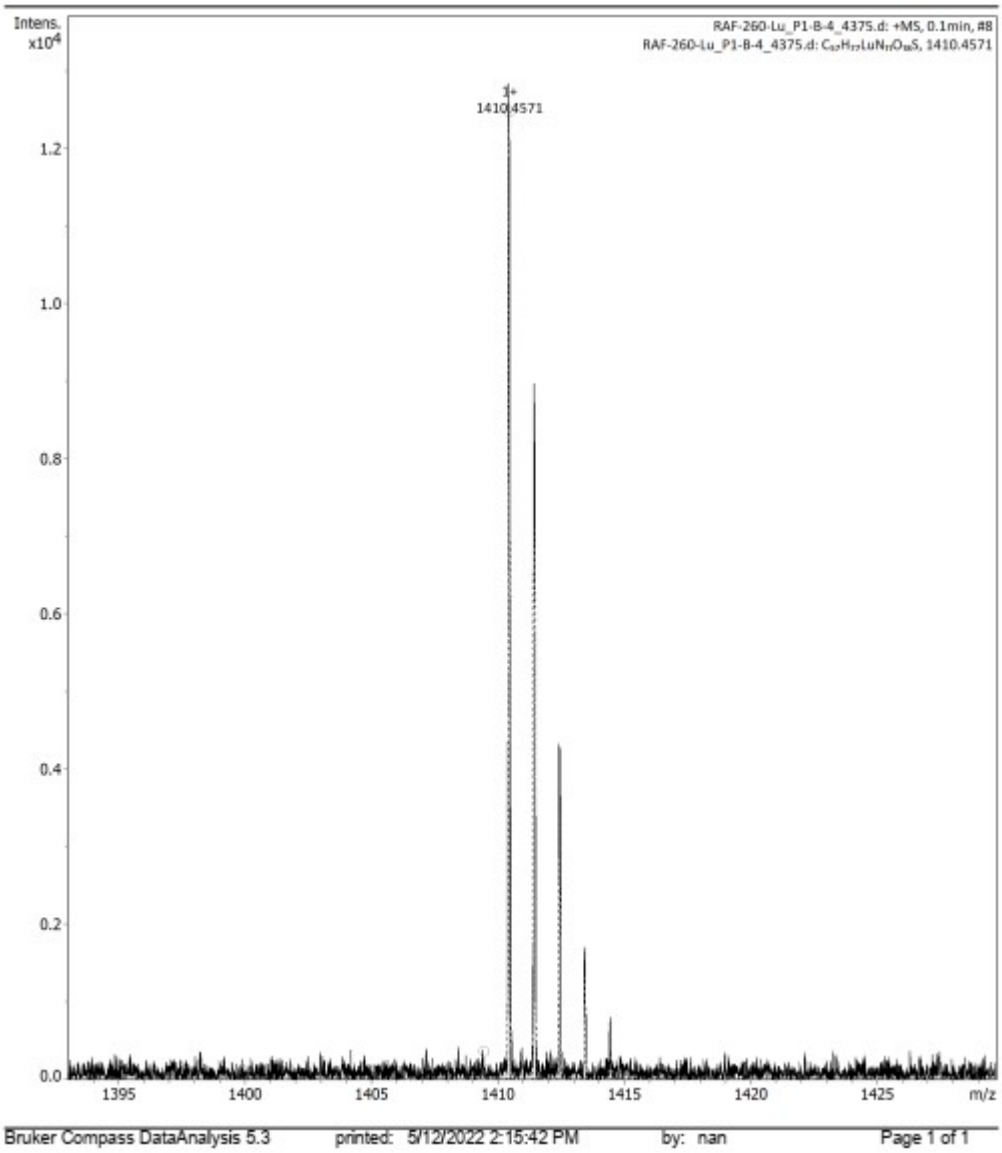

Figure S53: HR-ESI-MS of **[Lu(DO3Apic-SR$_2$)]**$^-$.

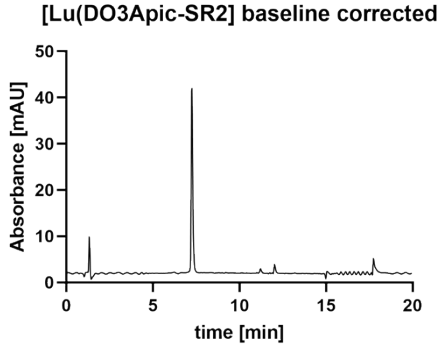

Figure S54: HPLC of **[Lu(DO3Apic-SR$_2$)]**$^-$.

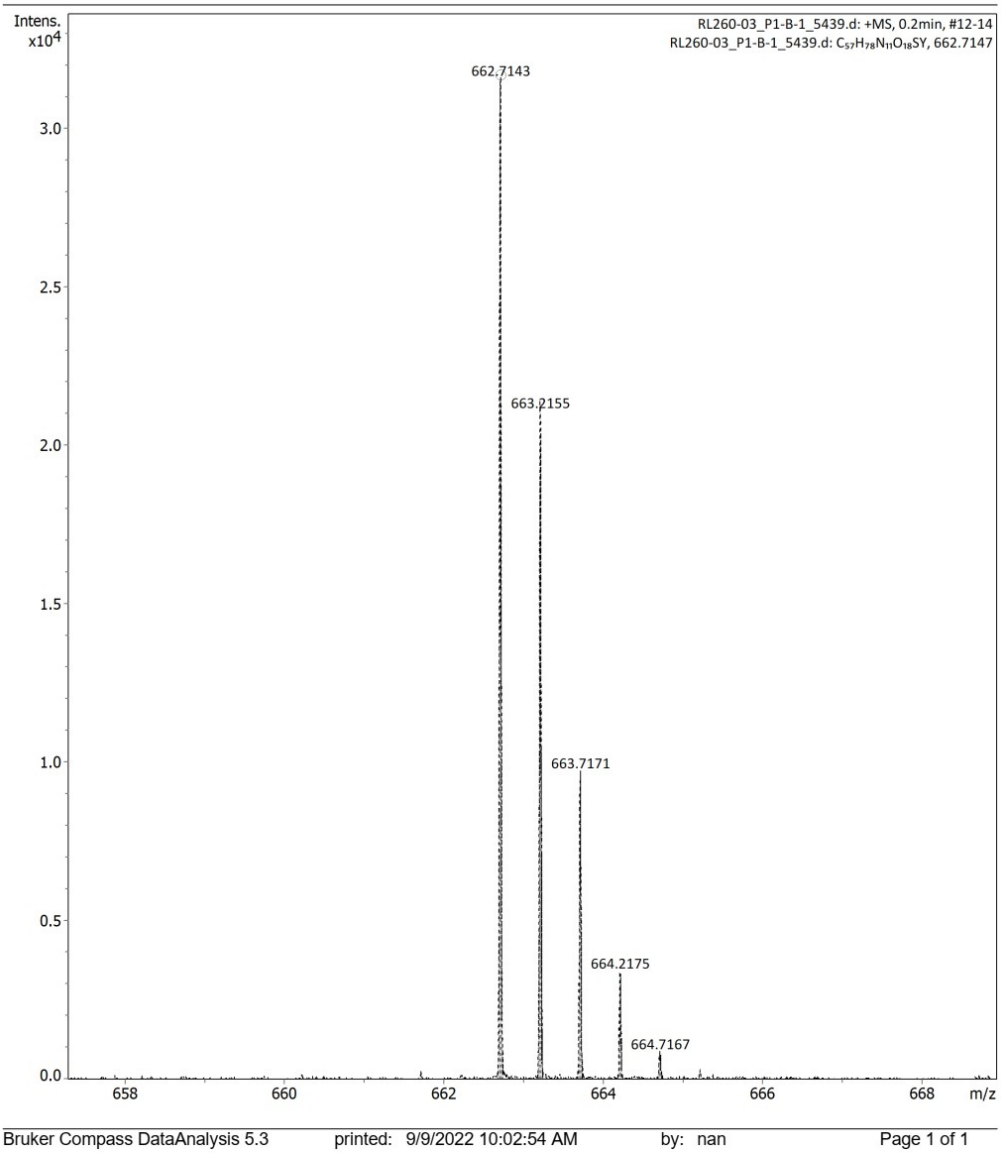

Figure S55: HR-ESI-MS of **[Y(DO3Apic-SR$_2$)]**$^-$.

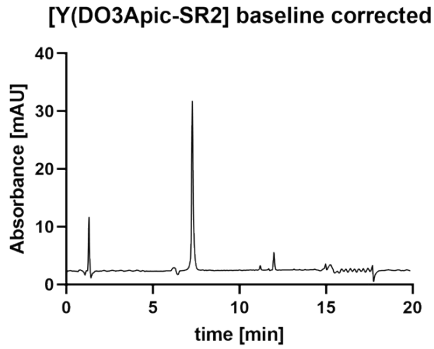

Figure S56: HPLC of **[Y(DO3Apic-SR$_2$)]**$^-$.

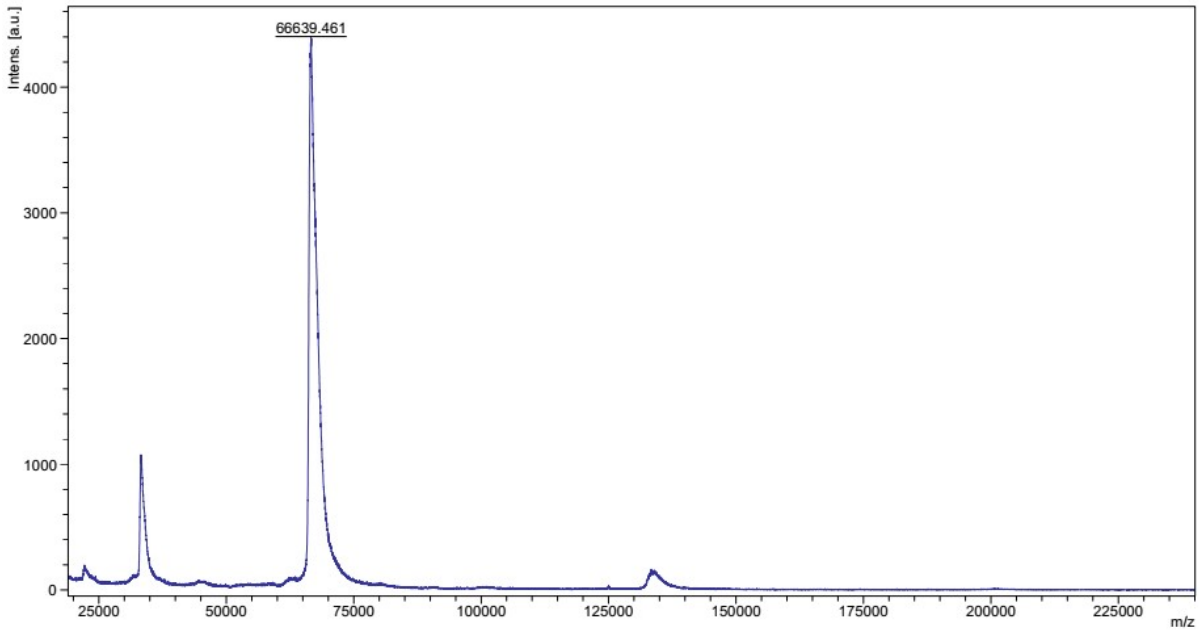

Figure S57: MALDI-TOF MS of BSA.

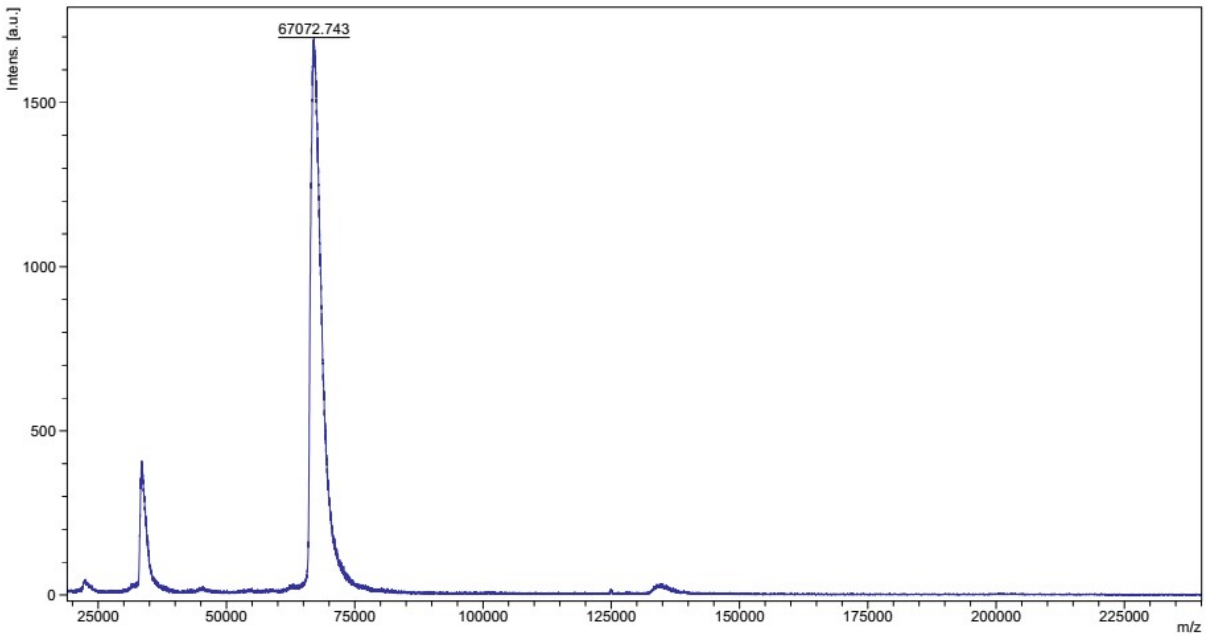

Figure S58: MALDI-TOF MS of BSA reacted with 100 equivalents of **[La(DO3Apic- NO_2)]**$^-$.

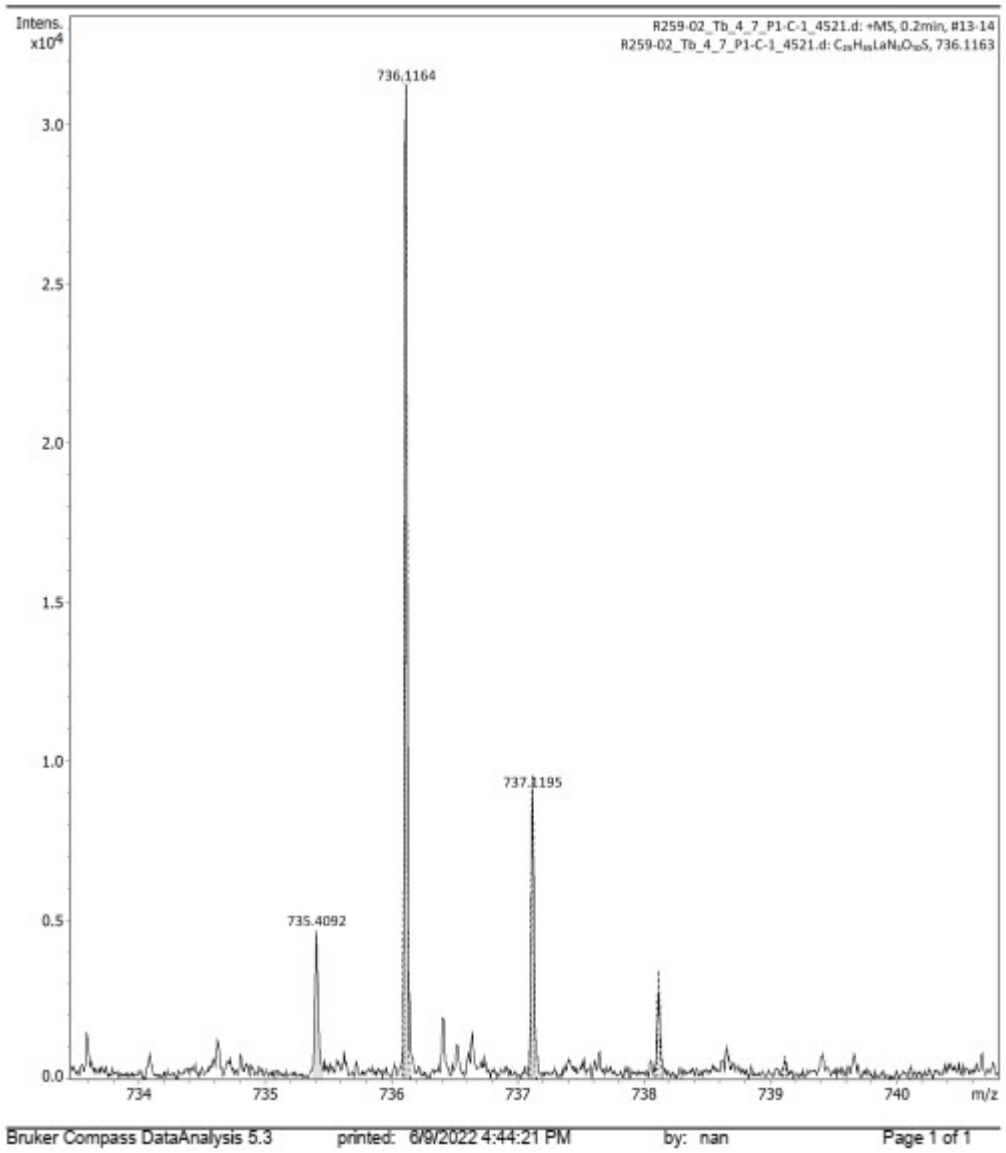

Figure S59: HR-ESI-MS of **[La(DO3Apic-SR$_1$)]**$^-$.

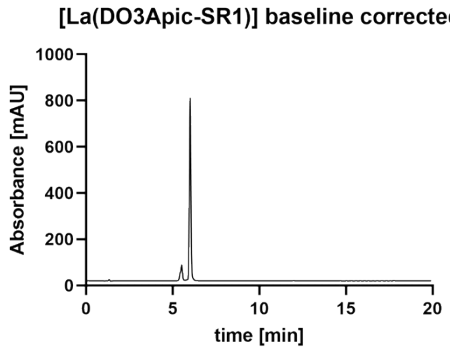

Figure S60: HPLC of **[La(DO3Apic- SR$_1$)]**$^-$.

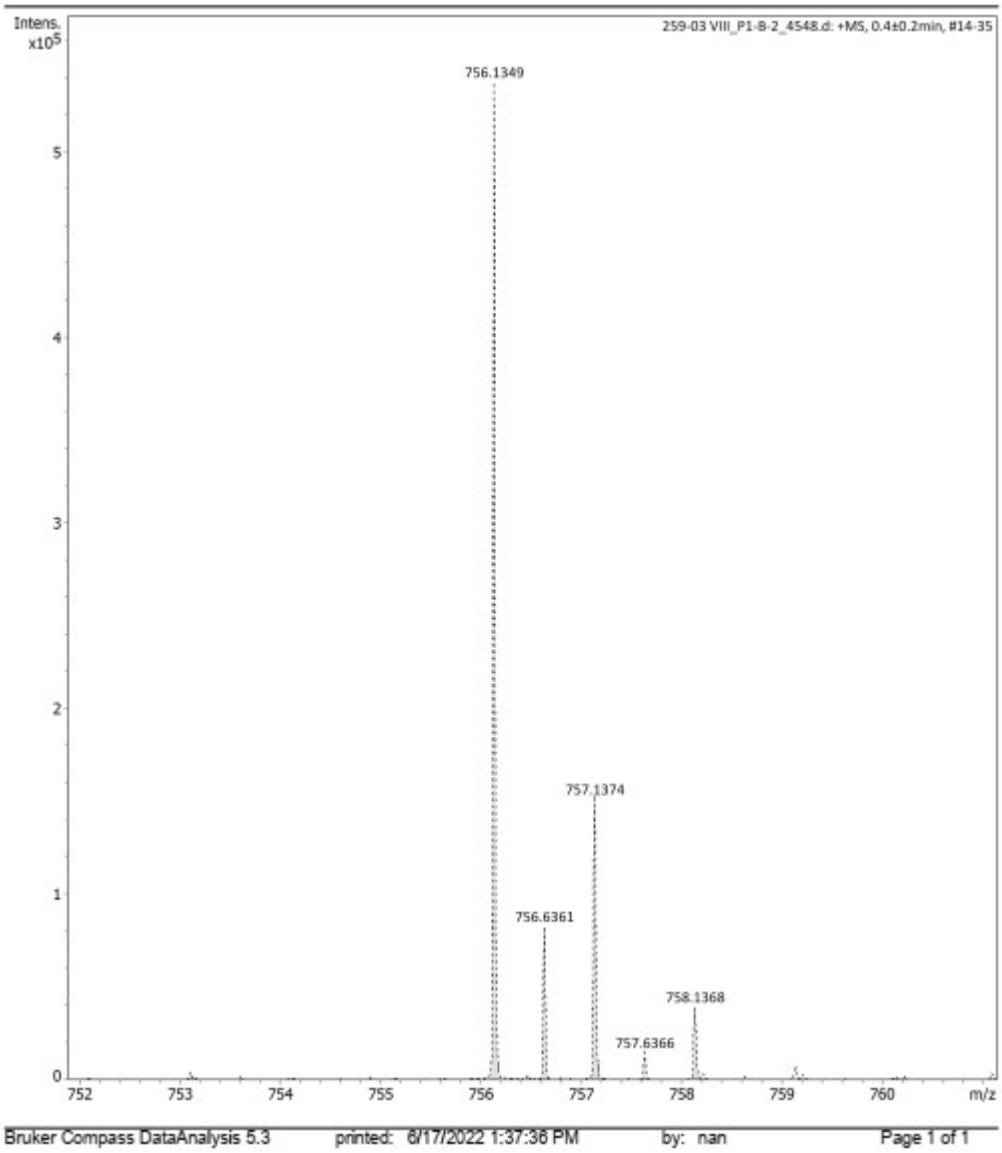

Figure S61: HR-ESI-MS of **[Tb(DO3Apic- SR_1)]**$^-$.

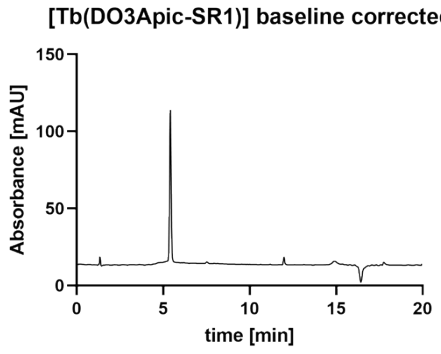

Figure S62: HPLC of **[Tb(DO3Apic- SR_1)]**$^-$.

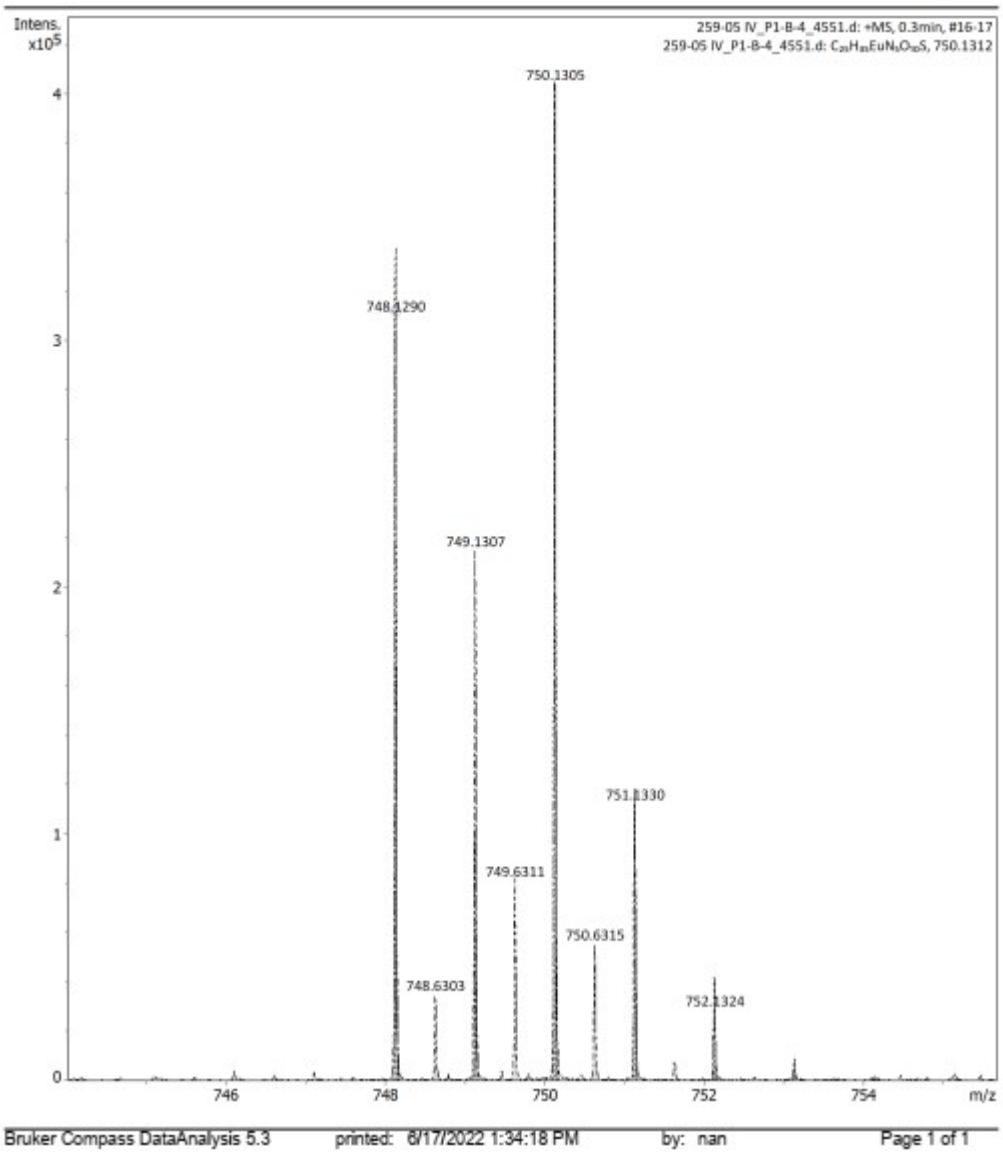

Figure S63: HR-ESI-MS of **[Eu(DO3Apic- SR_1)]**$^-$.

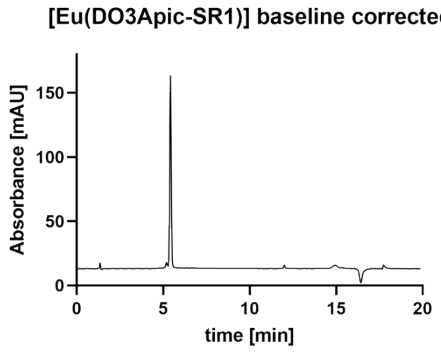

Figure S64: HPLC of **[Eu(DO3Apic- SR_1)]**$^-$.

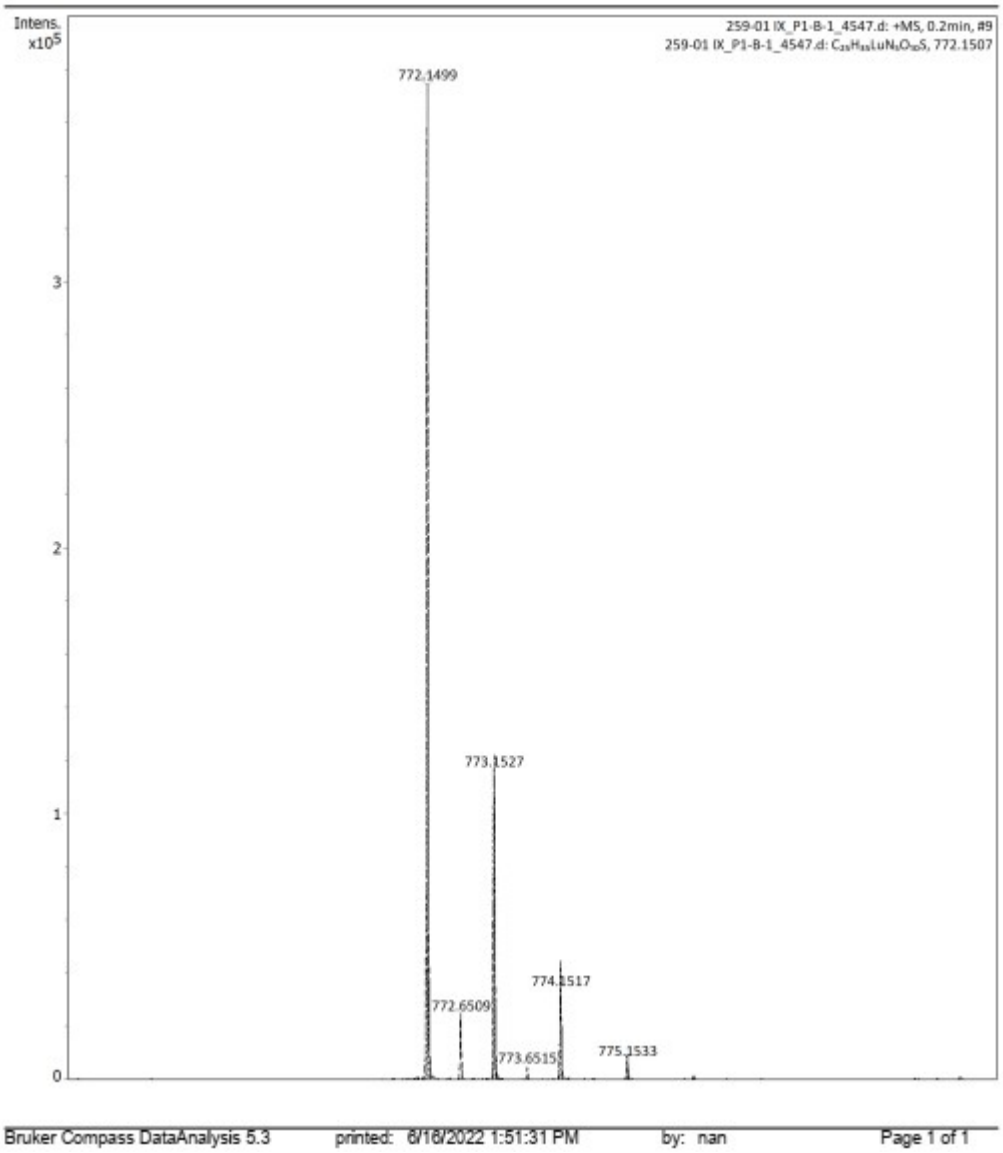

Figure S65: HR-ESI-MS of **[Lu(DO3Apic- SR_1)]**$^-$.

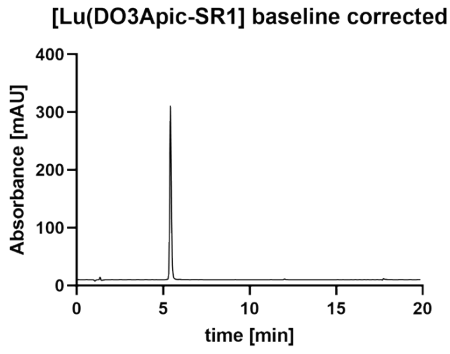

Figure S66: HPLC of **[Lu(DO3Apic- SR_1)]**$^-$.

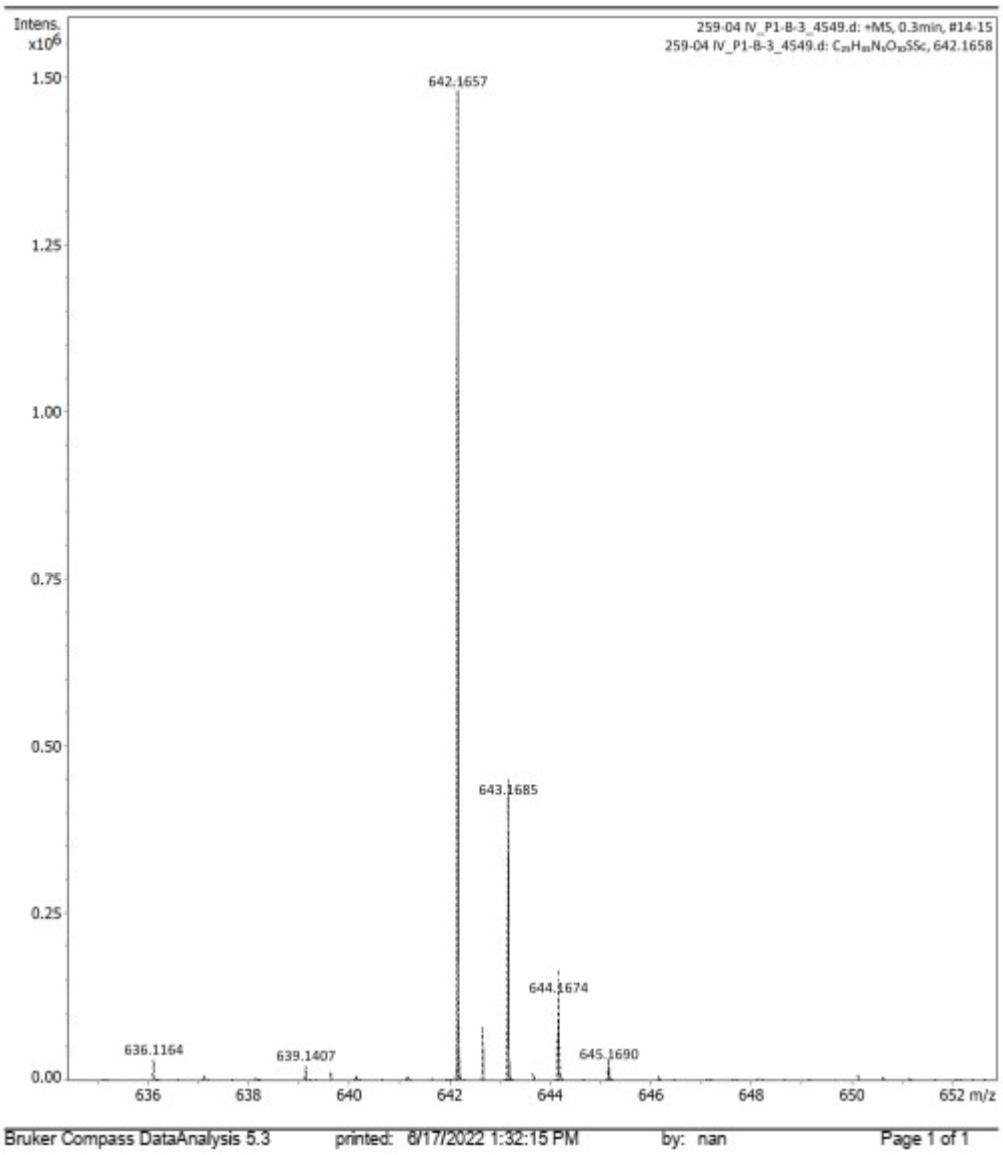

Figure S67: HR-ESI-MS of **[Sc(DO3Apic- SR_1)]**$^-$.

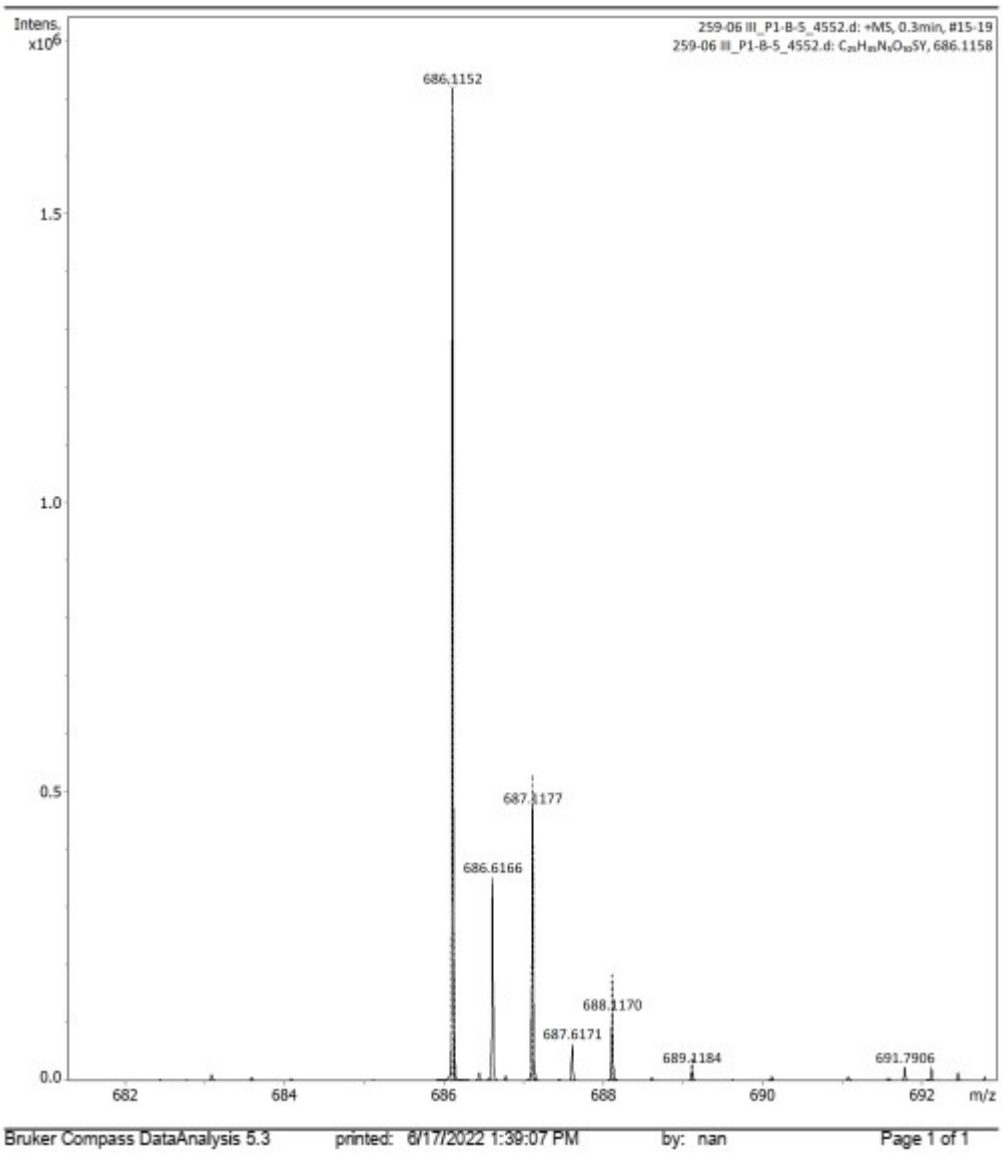

Figure S68: HR-ESI-MS of **[Y(DO3Apic- SR_1)]**$^-$.

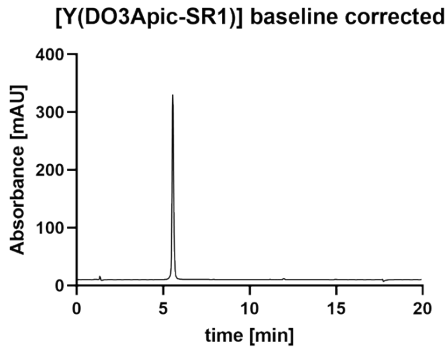

Figure S69: HPLC of **[Y(DO3Apic- SR_1)]**$^-$.

References

1. A. Shah, A. Roux, M. Starck, J. A. Mosely, M. Stevens, D. G. Norman, R. I. Hunter, H. El Mkami, G. M. Smith, D. Parker and J. E. Lovett, *Inorg. Chem.*, 2019, **58**, 3015-3025.
2. K. L. Gempf, S. J. Butler, A. M. Funk and D. Parker, *Chem. Commun.*, 2013, **49**, 9104-9106.
3. A. Beeby, I. M. Clarkson, R. S. Dickins, S. Faulkner, D. Parker, L. Royle, A. S. de Sousa, J. A. Gareth Williams and M. Woods, *J. Chem. Soc., Perkin Trans. 2*, 1999, DOI: 10.1039/A808692C, 493-504.
4. A. G. Cosby, S. H. Ahn and E. Boros, *Angew. Chem. Int. Ed.*, 2018, **57**, 15496-15499.